Oceanographic setting and short-timescale environmental variability at an Arctic seamount sponge ground

E.M. Roberts, F. Mienis, H.T. Rapp, U. Hanz, H.K. Meyer, A.J. Davies

www.elsevier.com

PII: S0967-0637(18)30025-6
DOI: https://doi.org/10.1016/j.dsr.2018.06.007
Reference: DSRI2924

To appear in: *Deep-Sea Research Part I*

Received date: 19 January 2018
Revised date: 8 May 2018
Accepted date: 11 June 2018

Cite this article as: E.M. Roberts, F. Mienis, H.T. Rapp, U. Hanz, H.K. Meyer and A.J. Davies, Oceanographic setting and short-timescale environmental variability at an Arctic seamount sponge ground, *Deep-Sea Research Part I,* https://doi.org/10.1016/j.dsr.2018.06.007

Oceanographic setting and short-timescale environmental variability at an Arctic seamount sponge ground

E.M. Roberts[a], F. Mienis[b], H.T. Rapp[c], U. Hanz[b], H.K. Meyer[c], and A.J. Davies[a]

[a] School of Ocean Sciences, Bangor University, Menai Bridge, Anglesey LL59 5AB, UK

[b] NIOZ Royal Netherlands Institute for Sea Research and Utrecht University, Department of Ocean Sciences, P.O. Box 59, 1790 AB Den Burg, Texel, The Netherlands

[c] Department of Biology and K.G. Jebsen Centre for Deep Sea Research, University of Bergen, P.O. Box 7803, N-5020 Bergen, Norway

Abstract

Mass occurrences of large sponges, or 'sponge grounds', are found globally in a range of oceanographic settings. Interest in these grounds is growing because of their ecological importance as hotspots of biodiversity, their role in biogeochemical cycling and bentho-pelagic coupling, the biotechnological potential of their constituent sponges, and their perceived vulnerability to physical disturbance and environmental change. Little is known about the environmental conditions required for sponges to persist and for grounds to form, and very few studies have explicitly characterised and interpreted the importance of oceanographic conditions. Here, results are presented of the first observational oceanographic campaign at a known sponge ground on the Schultz Massif Seamount (SMS; Arctic Mid-Ocean Ridge, Greenland / Norwegian Seas). The campaign consisted of water column profiling and short-term deployment of a benthic lander. It was supported by multibeam echosounder bathymetry and remotely operated vehicle video surveys. The seamount summit hosted several environmental factors potentially beneficial to sponges. It occurred within relatively nutrient-rich waters and was regularly flushed from above with slightly warmer, oxygen-enriched Norwegian Arctic Intermediate Water. It was exposed to elevated suspended particulate matter levels and oscillating currents (with diurnal tidal frequency) likely to enhance food supply and prevent smothering of the sponges by sedimentation. Elevated chlorophyll *a* concentration was observed in lenses above the summit, which may indicate particle retention by seamount-scale circulation patterns. High sponge density and diversity observed on the summit is likely explained by the combination of several beneficial factors, the coincidence of which at the summit arises from interaction between seamount geomorphology, hydrodynamic regime, and water column structure. Neighbouring seamounts along the mid-ocean ridge are likely to present similarly complex

oceanographic settings and, as with the SMS, associated sponge ground ecosystems may therefore be sensitive to changes over a particularly broad range of abiotic factors.

Keywords: Sponges, seamounts, mid-ocean ridge, deep sea, Hexactinellida, Astrophorida

1. Introduction

Mass occurrences of large sponges, or 'sponge grounds', are found globally, including in fjords, on continental shelves and slopes, and in the deep sea at mid-ocean ridges and seamounts (Barthel, 1992; Whitney et al., 2005; Hogg et al., 2010; Murillo et al., 2012; Bo et al., 2012; Cathalot et al., 2015; Maldonado et al., 2015). At sponge grounds, sponges dominate the benthic macrofauna in terms of body size and abundance (Hogg et al., 2010), and often account for the majority of invertebrate biomass (Klitgaard and Tendal, 2004; Murillo et al., 2012; Maldonado et al., 2015). Beyond this, considerable variability exists between prevailing 'types' of sponge ground (in terms of distribution, community composition, and species richness), and current understanding of these ecosystems is limited such that even a simple, quantitative framework of sponge ground definitions does not yet exist. Sponge grounds occurring in the deep sea have received relatively little scientific attention, in contrast to cold-water coral reefs, for example, which have been studied extensively in recent decades (see Freiwald and Roberts (2005)).

Interest in deep-sea sponge grounds has been growing, driven by three main factors. Firstly, sponges possess significant biotechnological and biomedical potential. Their anatomical structures have inspired biomimetic lines of research and their secondary metabolites are a valuable source of potentially useful bioactive compounds (e.g., Belarbi et al., 2003; Sundar et al., 2003; Ehrlich et al., 2010; Leal et al., 2012; Dudik et al., 2018). Secondly, sponge grounds are ecologically important. They are increasingly recognised as hotspots of biodiversity and biomass in the deep sea (Klitgaard, 1995; Beazley et al., 2013). They form complex biogenic habitats (sponge structures + 'spicule mat' substrate (Bett and Rice, 1992)), where there is a general paucity of such structural habitat (Buhl-Mortensen et al., 2010). These provide refuge, foraging, spawning, and nursery grounds for fish (Kenchington et al., 2013; Kutti et al., 2015), and create an abundance of microhabitats for sponge-associated invertebrates (Barthel, 1992; Bett and Rice, 1992; Herrnkind et al., 1997; Freese and Wing, 2003, and references therein; Henkel and Pawlik, 2005; Amsler et al. 2009; Maldonado et al., 2015). Sponge grounds also play important roles in biogeochemical cycling and bentho-pelagic coupling (Gatti, 2002; Pile and Young, 2006; Bell, 2008; Hoffmann et al., 2009; De Goeij et al., 2013; Kutti et al., 2013). Thirdly, deep-sea sponges are thought to be vulnerable to physical disturbance and environmental change (Hogg et al., 2010). This is in need of assessment to ensure adequate protection, mitigation, and sustainable exploitation measures are in place. Sponges may take millennia to form grounds (Murillo et al., 2016a), be very slow-growing (Pusceddu et al., 2014), and reproduce infrequently (Klitgaard and Tendal, 2004). Deep-sea sponge grounds have recently been

classified as a 'habitat under immediate threat and / or decline' by the OSPAR Commission (OSPAR, 2008), and a 'vulnerable marine ecosystem (VME)' by the Food and Agriculture Organisation of the United Nations (FAO, 2009).

Despite a growing body of research highlighting the functional significance of deep-sea sponge grounds, little is known about the environmental conditions required for sponges to persist, and for sponge grounds to form at specific locations. This is fundamentally important information for the assessment of their vulnerability and response to disturbance and climate change. Several authors have commented on the importance of various hydrographic variables. A number have emphasised the need for stable bottom conditions in terms of temperature and salinity (Klitgaard and Tendal, 2004; Murillo et al., 2016a), or relate the presence of sponges to that of a particular water mass or current system in the study region (Barthel et al., 1996, Klitgaard and Tendal, 2004; Murillo et al., 2012; Beazley et al., 2015; van Haren et al., 2017). Murillo et al. (2012) report the temperature and salinity ranges (3.38 – 3.84 °C; 34.85 – 34.90 ‰) experienced by sponge grounds dominated by large astrophorid demosponges off Newfoundland, Canada. They note that these conditions, provided by the Labrador Current, may be suitable for the sponges' persistence, but other factors must influence the finer-scale patterns of distribution in this region (Murillo et al. 2012). Modelling studies have implicated silicate concentration, and near-bed temperature and salinity (amongst other factors) as important drivers of broad-scale sponge ground distribution in the North Atlantic (Knudby et al., 2013; Howell et al., 2016). The availability of a suitable substrate for settlement, growth, and development seems likely to influence local-scale sponge distribution, though there is apparent variability in substrate requirements for different sponge species (Klitgaard and Tendal, 2004; c.f. Murillo et al., 2016a, 2016b). Water column turbidity has also been proposed as a factor limiting the distribution of sponge grounds (Klitgaard and Tendal, 2004). Excessive suspended particulate matter (particularly inorganic) loads are believed to clog the filtration systems of some sponges and therefore render some locations unviable for colonisation (Klitgaard and Tendal, 2004).

Hydrodynamical phenomena are frequently invoked as mechanisms explaining the presence of a sponge ground. Rice et al. (1990) considered the theoretical possibility that near-bed tidal currents are locally enhanced by interaction between the flow and the bed slope. A resonance-type intensification of the local currents is believed to occur at locations where internal tides (internal waves of tidal frequency) would typically be generated (Sandstrom, 1975; New, 1988; Huthnance, 1989), and it was hypothesised that these enhanced near-bed currents would resuspend (or maintain in near-bed suspension) flocculent phytodetrital material and improve food supply to a

downslope population of sponges (Rice et al., 1990). Different authors also place emphasis on the importance of internal tides, focussing instead on current enhancement by incident / reflecting internal tides propagating along water mass boundaries that impinge upon seabed features (e.g., slopes and seamounts), and the acceleration of local currents, the generation of turbulence, and the induction of various flow patterns by interactions between prevailing current regimes and irregular seabed topography have been proposed to be important at various spatial scales (Genin et al., 1986; Klitgaard and Tendal, 2004; McIntyre et al., 2016; van Haren et al., 2017). The importance of enhanced currents to sponge grounds is typically outlined in terms of improved food / larval supply and the prevention of smothering by settling suspended sediments. The idea that such currents are useful in inducing a passive flow through sponges that reduces the metabolic cost of pumping (Leys et al., 2011) has been thus far overlooked. Although sponge grounds are frequently found on sloped or irregular topography, leading to speculation about the predominance of hydrodynamic influence, McIntyre et al. (2016) note that they are also reported from relatively flat areas (e.g., Tromsøflaket in the Western Barents Sea (Klitgaard and Tendal, 2004; and personal observation) and Hatton Basin in the Northeast Atlantic (Durán Muñoz et al., 2011)).

Very few studies have explicitly set out to characterise and interpret the importance of oceanographic conditions at deep-sea sponge grounds. Genin et al. (1986) measured the current regime at the Jasper Seamount in the Eastern Pacific, which hosts an abundant and diverse fauna dominated by suspension feeders such as sponges and corals. They noted that abundance peaked at sites of flow acceleration (i.e., at topographic peaks), and they attributed this to flow conditions that are favourable either through a 'settlement pathway' (i.e., an enhanced supply of larval recruits per unit time) or a 'feeding pathway' (i.e., an enhanced supply of potential food per unit time) (Genin et al., 1986). White (2003) measured currents in the Porcupine Seabight (west of Ireland) at both locations of sponge presence and absence. Their measurements supported the hypothesis of Rice et al. (1990) that the sponges (the hexactinellid *Pheronema carpenteri*) favour locations adjacent to regions of enhanced near-bed tidal currents (where they benefit from the advection of resuspended material in the bottom boundary layer), but probably cannot tolerate the highest currents found locally (White, 2003). Whitney et al. (2005) examined the oceanographic conditions at hexactinellid sponge reefs occurring at the heads of shelf canyons off Canada's west coast. These authors identified up-canyon transport of water rich in nutrients (particularly silicates) and suspended matter as important in explaining sponge reef presence, and noted that conditions may be favourable in several other respects also (e.g., appropriate ranges of dissolved oxygen, temperature, and salinity, and the prevalence of moderate, tidally-modulated near-bed currents that increase

food supply to, and food residency times near, the sponges and prevent smothering by sedimentation) (Whitney et al., 2005). Beazley et al. (2015) investigated the hydrographic conditions associated with dense sponge grounds on the Sackville Spur in the Northwest Atlantic and concluded that their presence could potentially be attributed to a warm, salty remnant of the Irminger Current residing over the slope in that area.

No comprehensive oceanographic survey studies of deep-sea sponge ground localities currently exist for the Northeast Atlantic - Arctic region, despite there being numerous, widely distributed sponge grounds in the area (Klitgaard and Tendal, 2004). Such studies, though descriptive, offer valuable insight into the physical setting and environmental requirements of marine ecosystems. Studies of this type relating to cold-water coral reefs, for example, have identified food supply mechanisms (Davies et al., 2009; 2010) and improved understanding of the ideal conditions for their growth and development (Mienis et al., 2007). The purpose of the current paper is to present the results of the first short-duration, high temporal resolution, observational oceanographic campaign at a cold-water sponge ground (*sensu* Klitgaard and Tendal (2004)) on the Schultz Massif Seamount (SMS) of the Arctic Mid-Ocean Ridge. The campaign consisted of a water column profiling survey and a c. 3 day deployment of a benthic lander, and was supported by multibeam echosounder bathymetry and remotely operated vehicle (ROV) video data collection. The oceanographic setting and short-timescale environmental variability experienced by the sponges is described. A peak in sponge density and diversity was observed towards the seamount summit, and explanations for this observation are considered in light of the oceanographic data collected.

2. Materials and methods

2.1. Study site

The Schultz Massif (73° 50' N, 7° 34' E) is a seamount located at the Arctic Mid-Ocean Ridge (AMOR), a 4000 km long, ultraslow-spreading ridge extending northwards from north of Iceland into the Polar Basin (Bruvoll et al., 2009). It is situated at a bend in the ridge at which the Mohn Ridge transitions into the Knipovich Ridge (Fig. 1(a)). It has a broadly elliptical shape in plan view, with its major axis oriented northeast-southwest (Fig. 1(b)), and rises from abyssal depths of more than 2500 m in adjacent basins to depths of 560-600 m at the summit. A trough of approximately 100 m depth and 500 m width bisects the summit and is aligned with the major axis described above. The lower slope of the seamount is dominated by soft sediments (mainly calcareous foraminifera) with some rocky outcrops and areas covered by pillow lavas. At intermediary parts of the slope soft sediments are still dominant, but rocky outcrops and walls are common. Approaching the summit there are still some rocky outcrops; sediments have a high content of sponge spicules. In the upper 100 m of the seamount a spicule mat is present that is up to 20 cm thick.

Estimating the seamount's dimensions is complicated by it belonging to a ridge system. Based on bathymetry data collected (Fig. 1(b)), a major axis of 10 km and a minor axis of 4 km appear appropriate. The deepest contours relating to this footprint are 1400 -1500 m deep. We use these values in later calculations. However, they represent lower bound estimates and larger values could also be considered appropriate (e.g., 15 km x 6 km, >2000 m depth at the base), based on coarser resolution bathymetry datasets and depending on the criteria applied to define the seamount's extent. The effects of using larger estimates in calculations have been considered (see *Discussion*).

The SMS lies at the nominal boundary between the Greenland and Norwegian Seas, two of the three Nordic Seas (the Iceland Sea being the third). These seas host two-way advective exchange between the Polar Sea and the North Atlantic Ocean, and they act as primary sites of water mass formation and transformation, producing waters that feed into the deep North Atlantic Ocean as dense overflows across the Greenland-Scotland Ridge (Dickson and Brown, 1994; Mauritzen, 1996; Hansen and Østerhus, 2000). The physical oceanography of the Nordic Seas is described in Hopkins (1991), and the surface circulation is fairly well known. Polar Water, of low temperature and salinity, enters the region primarily as a surface water mass (Greenland Polar Water) in a southward flowing current (the East Greenland Current) that travels through the western side of the Fram Strait and along the eastern Greenland Shelf (Hopkins, 1991). North Atlantic Water, which is warmer and of higher

salinity, enters from the south, also as a surface water mass (Norwegian Atlantic Water, NwAtW), in the northwards flowing and variously branched Norwegian Atlantic Current (Orvik and Niiler, 2002). Nordic Sea water masses can thus be considered mixtures of Polar Water, North Atlantic Water, and locally-formed / -modified deep water(s) (Carmack and Aagaard, 1973). Key water masses in the vicinity of the SMS are likely to include Norwegian Deep Water (NwDW), Upper Norwegian Deep Water (uNwDW), Norwegian Arctic Intermediate Water (NwArIW), and NwAtW (defined above), though the influence of Greenland Basin water masses cannot be ruled out (Hopkins, 1991). Understanding of the circulation of intermediate and deep water masses is being continually revised, as more and better physical data become available. There is some evidence that Norwegian intermediate and deep water masses have an advective origin (i.e., as opposed to significant local production), in contrast to those in the Greenland and Iceland Seas (Hopkins, 1991; Jeansson et al., 2017).

The AMOR is a significant bathymetric feature in the Nordic Seas. It influences circulation patterns and water exchange between adjacent basins / seas (Mauritzen, 1996). Orvik and Niiler (2002) demonstrated that the western-most branch of the Norwegian Atlantic Current consists of a jet steered by topography such as the Mohn and Knipovich Ridges (Orvik and Niiler, 2002). The SMS is a prominent feature in the ridge system, and is likely to be subject to (and contribute towards the creation of) a complex oceanographic setting. It may be influenced by such topographically-steered deep currents. Hydrodynamical modelling efforts have predicted that semi-diurnal tidal constituents dominate diurnal constituents in terms of tidal elevation in the vicinity of the SMS (Lyard, 1997). In terms of tidal current velocity the reverse situation can occur, with diurnal tidal currents dominating (Kowalik and Proshutinsky, 1993, and references therein). Several of these authors note strong local responses to diurnal tidal forcing in the velocity field of the Northeast Atlantic - Arctic region. Harmonic constants and tidal predictions (elevations and currents) determined for the SMS from regional barotropic inverse tidal solutions using the Oregon State University Tidal Inversion Software (OTIS; Egbert and Erofeeva, 2002) corroborate the importance of diurnal tides to the velocity field (see *Results* and *Supplementary material*).

The sponge ground at the SMS has been the subject of several research cruises by the University of Bergen (UiB) since 2008. Biological sampling by means of ROV, epibenthic sledges, bottom trawls, and cores, supported by high-definition video imagery, has revealed seemingly rich and undisturbed benthic communities dominated mostly by sponges, anthozoans, and ascidians (see Torkildsen

(2013), as well as Cárdenas et al. (2013), Hestetun et al. (2017), and Plotkin et al. (2017) for dominating sponge taxa).

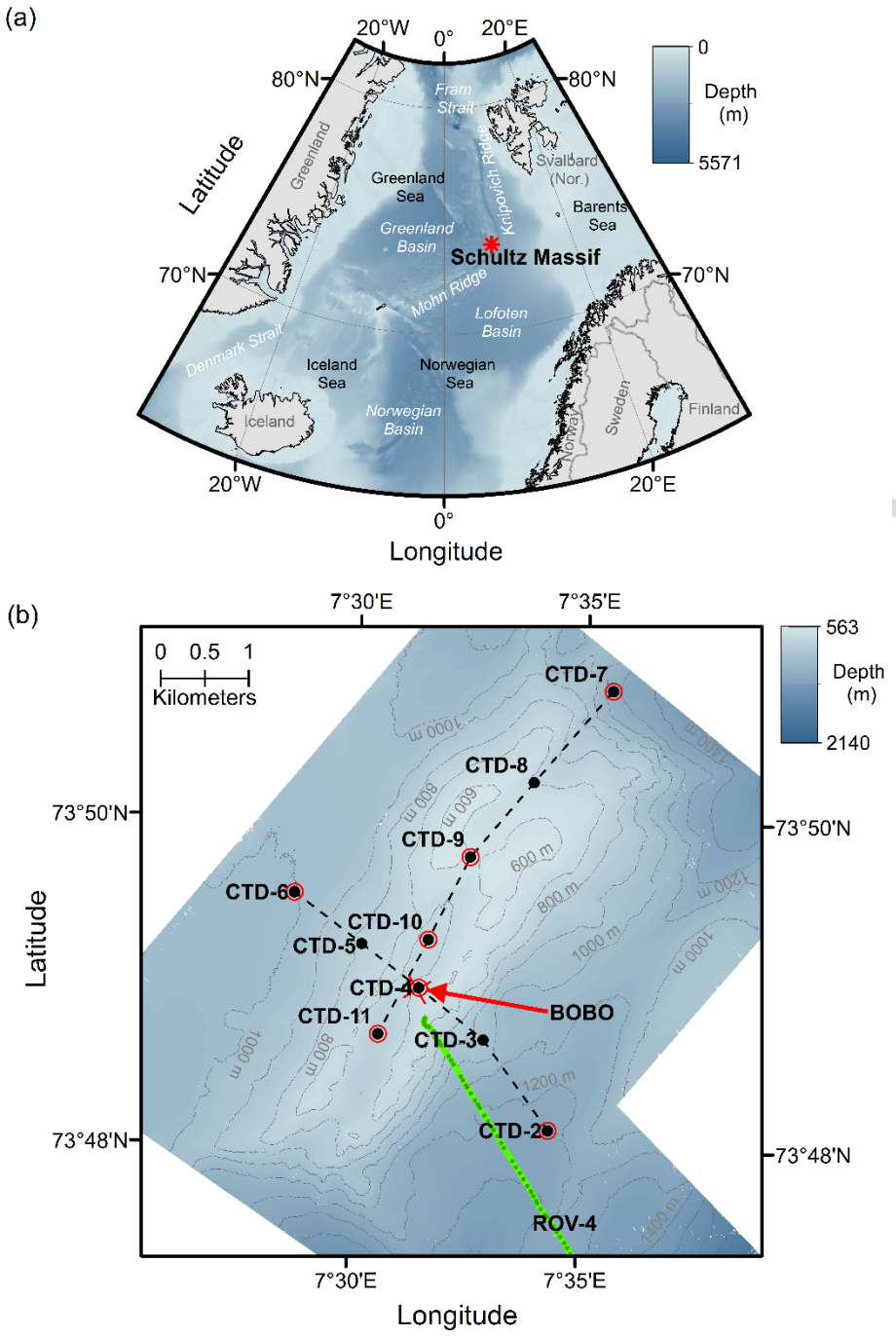

Figure 1 – The Schultz Massif Seamount (SMS) study site. (a) shows the location of the SMS in the Nordic Seas region (polar stereographic map projection; 30 arc-second bathymetry from General Bathymetric Chart of the Oceans 2014 (Weatherall et al., 2015); coastline data from NOAA's Global Self-consistent, Hierarchical, High-resolution Shoreline Database (Wessel and Smith, 1996)). (b) shows bathymetry at the SMS from multibeam echosounder data (EM 302; spatial resolution = 10 m). Conductivity, temperature, and depth (CTD) profile stations are indicated by solid black circles, and transects by dashed lines. Water sampling (rosette sampler) is indicated with additional red outer circles. The Bottom Boundary Benthic Lander (BOBO) is denoted by a red

cross. The bright green line shows the ROV video transect analysed; darker green dots indicate the positions of still images extracted for the analysis.

2.2. Fieldwork campaign

A multi-disciplinary research cruise to the SMS was conducted using the *RV G.O. Sars* (Norwegian Institute of Marine Research and UiB) from 18th to 26th June 2016. The present study focusses on physical and biogeochemical data collected during this cruise, particularly those from the deployment of a benthic lander and from water column profiling and sampling. Acoustic maps of the seamount bathymetry and high-definition video imagery of its benthic environments and fauna (captured using an ROV) have been used primarily to supplement existing knowledge on the site.

2.2.1. Acoustic mapping

The bathymetry of the SMS was mapped using an EM 302 multibeam echosounder system (Kongsberg Maritime AS, Kongsberg, Norway). The EM 302 has a nominal sonar frequency of 30 kHz and uses 288 beams (per swath) over a maximum angular coverage of 150° (beam spacing was equidistant). This system is well suited to mapping bathymetry in deep water, down to depths of 7000 m. Mapping of the seamount summit and flanks was achieved in four parallel survey lines (aligned approximately northeast to southwest), and the resulting bathymetric data (gridded to 10 m spatial resolution) were used to select a site for the benthic lander deployment and to plan the water column profiling survey strategy.

2.2.2. ROV video imagery and water sampling

ROV Ægir 6000 (Kystdesign AS, Haugesund, Norway) is a 95 kW remotely operated vehicle (dimensions: 2.75 x 1.70 x 1.65 m) rated to 6000 m water depth, owned by UiB. It has considerable scientific payload capacity (400 kg) and can be deployed with various suites of modular sensors and sampling equipment. High-definition video footage of benthic communities on the SMS was recorded during base-to-summit transects from several directions and during targeted biological sampling for taxonomic and other studies.

For the present work, imagery from video transect ROV-4 (see Fig. 1) was analysed. The transect ran approximately south-east to north-west, spanned a depth range of 1313 m to 658 m (i.e., approaching the summit), and took 8 h to complete. Still images were extracted from the footage at 5 min intervals and analysed to obtain estimates of species richness and abundance for the major taxonomic groups present amongst the large epifauna observed. ROV altitude (or 'flying height') varied over the transect. For consistency, images captured when ROV altitude was outside the range 1 - 3 m were not included in the analysis. 16 images were disregarded for this reason, out of 72 'under-way' images available. It was not possible to reliably provide quantities per unit area, but

values 'per image' are sufficient to demonstrate relative changes / trends over depth, as is required for this study (particularly for sponges (phylum Porifera) as a group). More in-depth analysis of the video transect data will be presented in a forthcoming publication.

The ROV was fitted with small Niskin bottles (3 L sample volumes), which were used to opportunistically sample water near the seamount summit. Sub-samples were taken for dissolved inorganic carbon and nutrient concentration analysis, and were handled according to the procedures outlined in section 2.4. below.

2.2.3. Near-bed observations

A free-falling, autonomous 'Bottom Boundary' Benthic Lander (BOBO; van Weering et al., 2000) was deployed near the seamount summit (73° 48.960' N, 7° 31.408' E, at 669 m water depth) on the 20th June 2016 for a period slightly longer than 3 days. It was equipped with instruments set to log time series observations of several key oceanographic parameters, including water temperature, salinity, dissolved oxygen concentration, and current velocity. In the present study, a short-leg lander configuration (i.e., relative to the original design) was employed.

The scientific payload of the BOBO Lander included the following instruments: (1) an SBE 16 Seacat conductivity and temperature (CT) Sensor (Sea-Bird Electronics Inc., Washington, USA), mounted at 2 metres above the seabed (mab) upon deployment; (2) a Rinko I fast response optical dissolved oxygen sensor (JFE Advantech Co. Ltd., Hyogo, Japan), mounted at 2 mab; (3) an upward-looking 300 kHz acoustic Doppler current profiler (ADCP) (Teledyne RDI Inc., California, USA), mounted at 2.2 mab; and (4) a high-definition video camera (Sony Corp., Tokyo, Japan) with LED illumination, directed at the seabed just outside the footprint of the lander and mounted at 0.7 mab. Sensors were programmed with a 5 min sampling interval, with the exception of the video camera, which was programmed to record 30 s of footage every 15 min.

The lander also hosted a programmable, autonomous particulate sampler (Phytoplankton Sampler (PPS), McLane Research Laboratories Inc., Massachusetts, USA). This was programmed to pump 24 individual *in situ* water samples, in time series, through pre-combusted, pre-weighed glass microfibre filters (47 mm diameter Whatman GF/F, nominal pore size 0.7 µm, GE Healthcare UK Ltd., UK) for the determination of suspended particulate matter (SPM) concentration by gravimetric analysis (after Strickland and Parsons, 1972). The programme was scheduled to begin shortly after lander deployment, with a sample volume of 7.5 L being filtered every 2 h at a flow rate of 125 mL

min^{-1}. Owing to battery failure and filter paper damage, only 10 reliable samples were obtained over the first 22 h and the resulting values were averaged to obtain a near-bed SPM estimate for comparison with water column concentrations.

2.2.4. Water column profiling

Water column profiling at the SMS was conducted along two transects: across the seamount's ridge-like summit, and along the summit ridge (Fig. 1(b)). Each transect consisted of 5 CTD stations. The across-ridge CTD transect commenced at 04:02 h UTC on the 22nd June 2016 at the south-eastern end of the transect (CTD-2 in Fig. 1(b)), and was completed by 09:06 h UTC. The along-ridge transect commenced at 07:18 h UTC on the 23rd June 2016 at the north-eastern end of the transect (CTD-7 in Fig. 1(b)), and was completed by 11:41 h UTC. Profiling was carried out using a conductivity, temperature, depth (CTD) system (SBE-9, manufactured by Sea-Bird Electronics Inc., Washington, USA) with additional sensors including a dissolved oxygen sensor (SBE-43, also by Sea-Bird), a turbidity sensor (Seapoint Sensors Inc., New Hampshire, USA), and a fluorometer (AquaTracka III, manufactured by Chelsea Technologies Group Ltd., UK). At all stations, the CTD unit was lowered to approximately 10 – 20 mab and raised before moving on to the next station. The CTD system was installed on a rosette water sampler (consisting of twelve 10 L Niskin water bottles). Water samples were collected at selected stations (those indicated by solid black circles with red outer rings in Fig. 1(b)) and depths (typically near-bed, mid-water column, and chlorophyll *a* maximum / surface) for a suite of analyses, including the determination of inorganic nutrient (PO_4^{3-}, NO_3^- + NO_2^-, Si), dissolved inorganic carbon (DIC), and suspended particulate matter (SPM) concentrations (see section 2.4.). CTD-1 was an off-seamount reference station, approximately 20 km to the southeast of the SMS (73° 38.896' N, 7° 52.734' E, 2462 m water depth), which was sampled (profiles and water samples) on the 20th June 2016 at 07:55 h UTC. All reported CTD depth values were estimated from measured pressures using equations from Fofonoff and Millard (1983).

2.3. Particle motion analysis of video footage

Owing to component failure within the ADCP, video footage from the lander was analysed instead to infer the nature of the current regime from recorded particle motion. 326 videos were captured sequentially over the course of the lander deployment. Each video was converted into 'stacks' of individual image frames (1920 x 1080 pixels), such that 300 frames were produced per video (i.e., 10 frames per second of footage). A smaller region (180 x 500 pixels) was extracted from the top right corner of each frame for further analysis, as this area consistently contained clearly identifiable particles.

Coordinates (in pixels from the image origin) and frame numbers were obtained for the start and end of the trajectories of up to 10 particles per video using the image processing software ImageJ (Schneider et al., 2012). Assuming linear paths and constant speeds, particle speeds and directions were calculated using Pythagoras' Theorem (for distance travelled, in pixels), frames elapsed (as a proxy for travel time), and trigonometric relations (to determine direction). Average particle speed was determined for each video by calculating the arithmetic mean of the individual particle speeds (i.e., scalar averaging), whilst average particle direction was determined as a unit vector average (see Gilhousen, 1987).

Average particle speeds were converted from units of 'pixels per frame' to relative units by normalising all values by the maximum observed over the deployment period. More meaningful physical units could not be obtained because the camera set-up lacked a means of determining spatial scale accurately (e.g., parallel lasers of known separation). Direction determined in the way described refers to particle motion occurring in the plane of the images only (i.e., no particle motion towards or away from the camera was quantified). We used the convention that 0° relates to vertical motion upwards, 180° relates to downwards motion, 90° relates to lateral motion towards the right of the image, and 270° relates to motion towards the left. It was not possible to relate these directions to a geographic coordinate system (e.g., to estimate flow direction).

Some qualitative criteria were applied to the selection of particles to analyse. Brighter, clearer particles were preferentially selected, as these could be more easily 'tracked'. Particles that exhibited an obvious change in diameter over their trajectories were deemed likely to possess a component of motion in the axis perpendicular to the plane of the image (i.e., towards or away from the camera) and were thus ignored (motion in this axis could not be resolved precisely). Any particles with curved or spiralling trajectories were ignored, since straight-line travel was assumed in calculations. Approximately 12% of the videos failed to provide 10 particle trajectories for analysis (the minimum number of trajectories analysed for any one video was 3).

2.4. Water sample analyses

In situ water samples were collected at several stations, as described in section 2.2.4. For every sampled depth, two times 5 L of seawater were immediately filtered over pre-combusted (450°C; 4 h), pre-weighed (balance precision = ±0.01 mg) GF/F filters (47 mm diameter; 0.7 µm nominal pore size) under an applied vacuum for the determination of SPM concentration by gravimetric analysis.

After filtration, filters were flushed with 100 mL of purified water to dissolve salt crystals, and were then stored at -20°C until further analysis at NIOZ. In the laboratory, filters were freeze-dried (~12 h; Vaco 5 (Zirbus Technology GmbH, Germany)) and re-weighed in order to calculate the total mass of suspended matter in each water sample.

Additional samples were taken from the Niskin bottles for the determination of dissolved inorganic carbon (DIC) and nutrient concentrations (i.e., phosphate (PO_4^{3-}), ammonium (NH_4^+ - not presented), nitrate (NO_3^-), nitrite (NO_2^-), and silicate (Si)). These were collected in 50 mL Nalgene bottles, which had been rinsed three times with water from the relevant Niskin bottles before filling. After sampling on deck, samples were filtered through 0.2 µm polycarbonate membrane filters (Whatman Nuclepore). Those samples intended for nutrient analysis were immediately sub-sampled into two vials, one of which was used for PO_4^{3-}, NH_4^+, NO_3^-, and NO_2^- determination (stored at -20°C) and the other for Si determination (stored at 4°C). Nutrient concentrations were determined by colorimetric analyses in the NIOZ laboratory using a QuAAtro Continuous Segmented Flow Analyser (Seal Analytical Ltd., UK). Measurements were made simultaneously on four channels: PO_4^{3-}, NH_4^+, NO_2^-, and NO_3^- and NO_2^- combined. Si concentrations were analysed in separate runs of the QuAAtro system. All measurements were calibrated against standards diluted to known nutrient concentrations with low nutrient seawater (LNSW). The LNSW was in the salinity range of the stations at the SMS (approximately 35 psu) to ensure calibration standards were of equivalent ionic strength to samples and hence negate salt effects. Each run of the system produced a calibration curve with a correlation coefficient of at least 0.9999 for 10 calibration points, but typically 1.0000 for linear chemistry. A freshly-diluted, mixed nutrient standard, containing silicate, phosphate, and nitrate (a so-called 'nutrient cocktail'), was measured in every run, as a guide to monitor the performance of the standards.

Filtered seawater samples intended for DIC determination were transferred into glass vials already containing 15 µL $HgCl_2$ (mercury chloride). The vials were filled with a convex meniscus before being capped and stored upside down in a refrigerator. Samples were analysed on a Traacs 800 Auto-Analyser (Seal Analytical Ltd., formerly Technicon) following the methodology described in Stoll et al. (2001).

3. Results

3.1. Sponge ground characteristics from biological sampling

Variation was observed in the composition and distribution of sponge-dominated communities along a depth gradient (i.e., summit, slope, and base) on the seamount. The summit and shallower areas (560 - 700 m water depth) were inhabited mainly by dense aggregations of hexactinellid sponges (*Schaudinnia rosea*, *Trichasterina borealis*, *Scyphidium septentrionale*, and *Asconema foliata*) (see also Torkildsen, 2013) along with tetractinellids (*Geodia parva*, *G. hentscheli*, and *Stelletta rhaphidiophora*) (Cárdenas et al., 2013) growing on a mixed substrate dominated by spicule mats (Fig. 2(a)). The slope was largely dominated by *G. hentscheli*, polymastiids, and various encrusting sponges growing on hard substrates (Fig. 2(b)). Deeper areas (>2000 m depth) were dominated by the demosponges *Spinularia sarsi*, *Tentorium semisuberites*, and *Thenea abyssorum* (Barthel and Tendal, 1993; Plotkin et al., 2017) on soft sediments, along with the hexactinellid sponges *Caulophacus arcticus* and *Asconema megaatrialia* and dense aggregations of unidentified Axinellidae on hard substrates (mainly pillow lava) (Torkildsen, 2013; this study, Fig. 2(c)). The dominating sponge fauna found on the SMS represent a core group of ground-forming species shared by a number of seamounts along this ridge system.

ROV video transect analysis (ROV-4) revealed trends of increasing species richness and total abundance with decreasing water depth (i.e., increasing elevation up the seamount) for the phylum Porifera (plots in Fig. 2), which clearly dominated the large epifauna. Similar trends were observed in ROV transects from different directions, and more in-depth analysis of these data will be presented in a forthcoming article. The summit sponge aggregations were particularly dense and diverse, and the seabed there is largely covered by surficial spicule mats of several centimetres thickness (~10 - 20 cm thick - data not presented in this article).

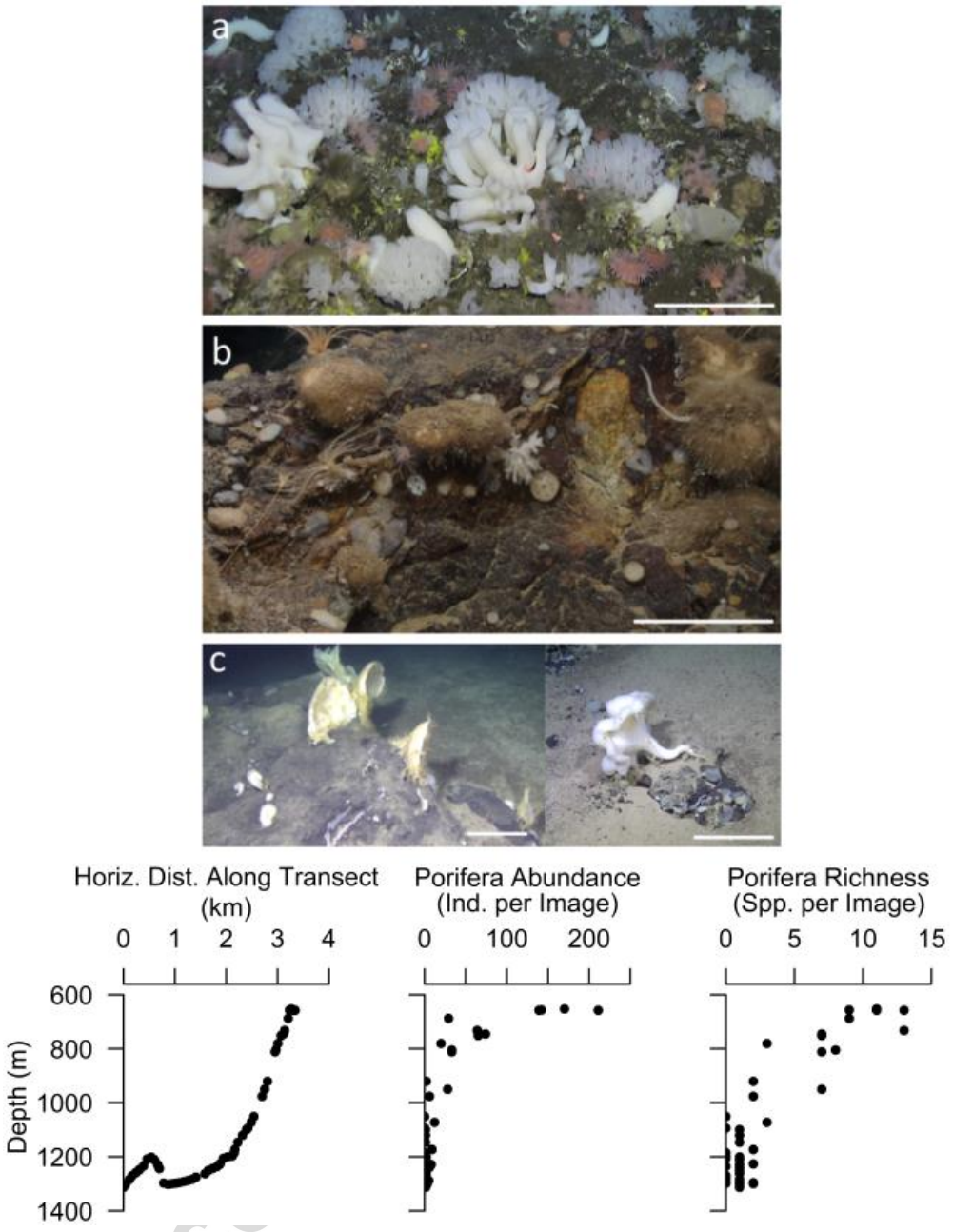

Figure 2 – Sponge-dominated communities found along a depth gradient on the Schultz Massif Seamount. (a) shows the typical sponge community in the summit area (560 - 700 m depth), dominated by *Schaudinnia rosea* (coarse branching sponge) and *Asconema foliata* (delicate branching sponge) growing on a dense layer of spicule mat and living tetractinellid sponges (*Geodia parva*, *G. hentscheli*, and *Stelletta rhaphidiophora*). (b) shows the seamount flank (at ~1000 - 1400 m depth), dominated by *Geodia hentscheli* (brownish, massive) and the polymastid *Spinularia njordi* (disc-shaped). (c) shows an unidentified Axinellidae (left) and *Caulophacus arcticus* (right), two common representatives of the sponges found on hard substrates in deeper areas around the base of the seamount. All scale bars represent 0.3 m. Plots beneath the images show depth profiles of total abundance and species richness of sponges (phylum Porifera), as determined from ROV video transect analysis.

3.2. Oceanographic setting from water column profiling

Representative water depth profiles of key oceanographic parameters are shown in Fig. 3. Profiles were similar across all seamount stations (i.e., CTD-2 to -11). A permanent thermocline and halocline are clearly discernible in panels (a) and (b), respectively, between approximately 200 and 400 m. There is also evidence of seasonal stratification occurring near the surface.

Dissolved oxygen concentration (Fig. 3(d)) exhibited a sub-surface maximum in the upper water column (~25 m depth). This was coupled with maxima in both fluorescence and turbidity (panels (e) and (f)), suggesting a productive surface layer most likely benefitting from oxygenated water and, at least in its upper range, light availability. A broad zone of reduced oxygen concentration was present, centred on the base of the surface layer (~200 m). Below this zone, a layer of elevated oxygen concentration was observed between 300 and 650 m. Within the oxygen-enriched layer, a peak in oxygen concentration was consistently observed to coincide approximately with the level of the adjacent seamount summit. Spatio-temporal variability in the position of this peak over the survey is illustrated in Fig. 3(d) by the inclusion of oxygen profiles from a number of other CTD stations.

In several profiles (particularly CTDs 3, 4, and 7-11), secondary peaks in fluorescence were apparent at the upper boundary of the oxygen-enriched layer (~300 m; Fig. 3(e)). Close inspection reveals associated peaks in turbidity (Fig. 3(f)), likely indicating the presence of a lens (or lenses) of water with elevated suspended matter content or a thin intermediate nepheloid layer (INL). No similar features were observed at the off-seamount reference station (CTD-1). Note that the turbidity profile in Fig. 3(f) has been smoothed to remove spikes caused by large individual particles and/or instrument noise. Profiles of chlorophyll *a* concentration and turbidity are shown together for all CTD stations in supplementary Figs. S1 and S2. High surface values have been omitted (i.e., 200 - 1000 m depth plotted) to allow the use of an appropriate horizontal axis scale for inspecting the smaller, secondary peaks. The square of the Brunt-Väisälä buoyancy frequency, N^2 (a measure of stratification stability), is also shown. The chlorophyll and turbidity peaks at ~300 m coincide with peaks in N^2. The lenses of suspended matter appear to have occurred at a local increase in vertical density gradient (also seen in Fig. 3(c)) associated with the transition to the oxygen-enriched layer / intermediate water mass.

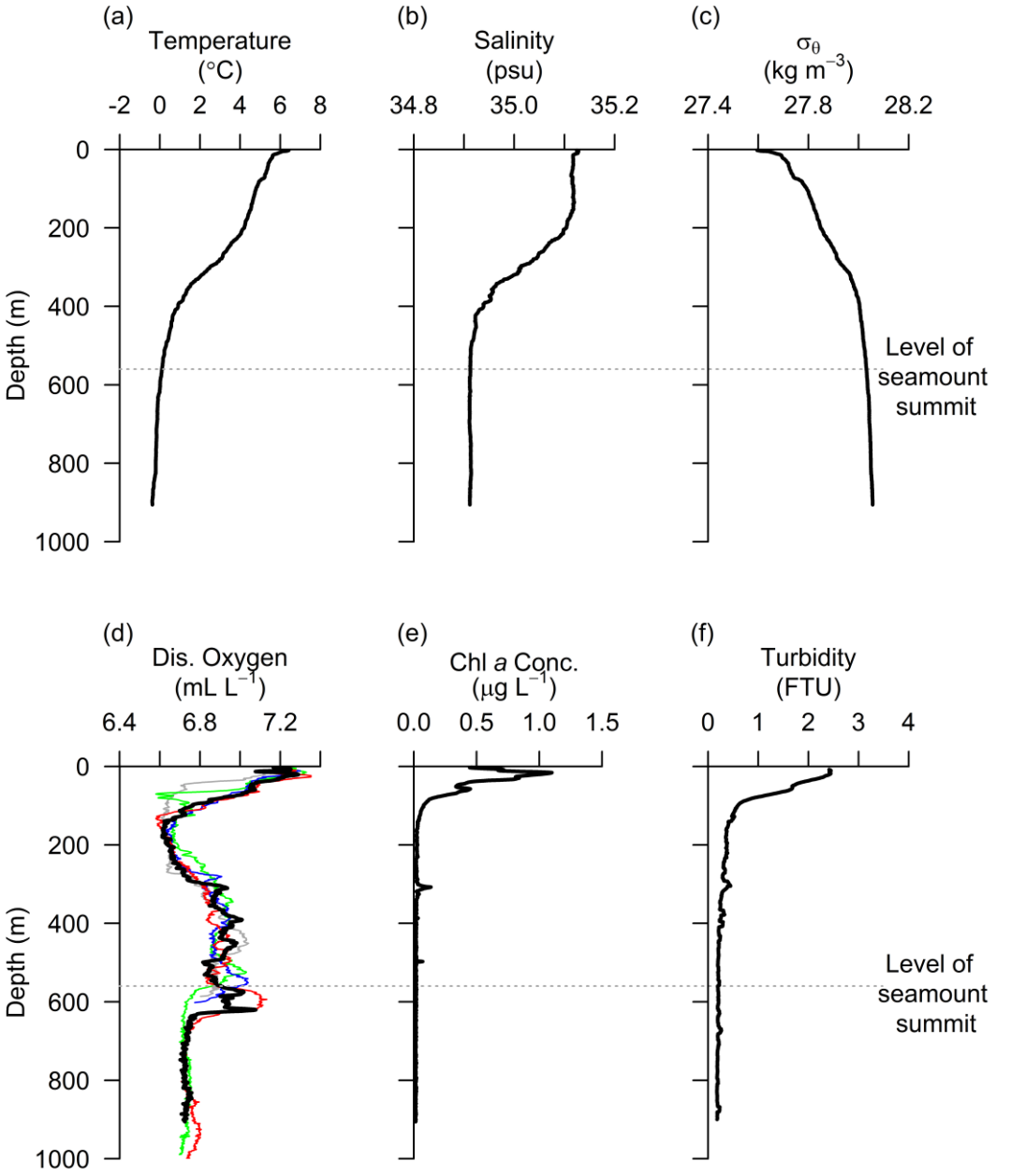

Figure 3 - Vertical profiles of (a) water temperature, (b) salinity, (c) potential density anomaly (σ_θ), (d) dissolved oxygen concentration, (e) chlorophyll *a* concentration, and (f) turbidity from CTD Station 3. Dissolved oxygen profiles from several other CTD stations are also plotted in panel (d) (coloured lines) to illustrate the variability observed in the position of the local maximum near the level of the seamount summit.

The permanent thermocline and halocline were also observed at approximately 200 – 400 m depth in the across-ridge CTD transect (Fig. 4(a) and (b)). The oxygen-enriched layer, apparent in Fig. 3, spans the entire transect and has a near-constant thickness of approximately 300 m (Fig. 4(c)). The lower boundary of this layer was just above the level of the bed (at the ridge crest), though the transect did not cross the absolute summit of the seamount, which was almost 100 m shallower. Lenses of water with elevated fluorescence levels are evident above the ridge crest (Fig. 4(d)) at the upper boundary of the oxygen-enriched layer. Cross-sections from the along-ridge CTD transect exhibit similar features and are shown in Fig. 5. Notably this transect bisected the seamount summit, crossing topography of greater elevation, and so convergence of the oxygen-enriched layer upon the summit is apparent. In both cross-sections there is evidence of the vertical displacement of isotherms in the mid-water column (~300 – 600 m) from station to station. Such displacements indicate either a modification of the water column structure by the seamount or baroclinic tidal perturbations captured over the course of each CTD transect. In the along-ridge salinity and dissolved oxygen cross-sections (Fig. 5(b) and (c)) horizontal gradients present in surface waters (< 200 m) may indicate a frontal scenario.

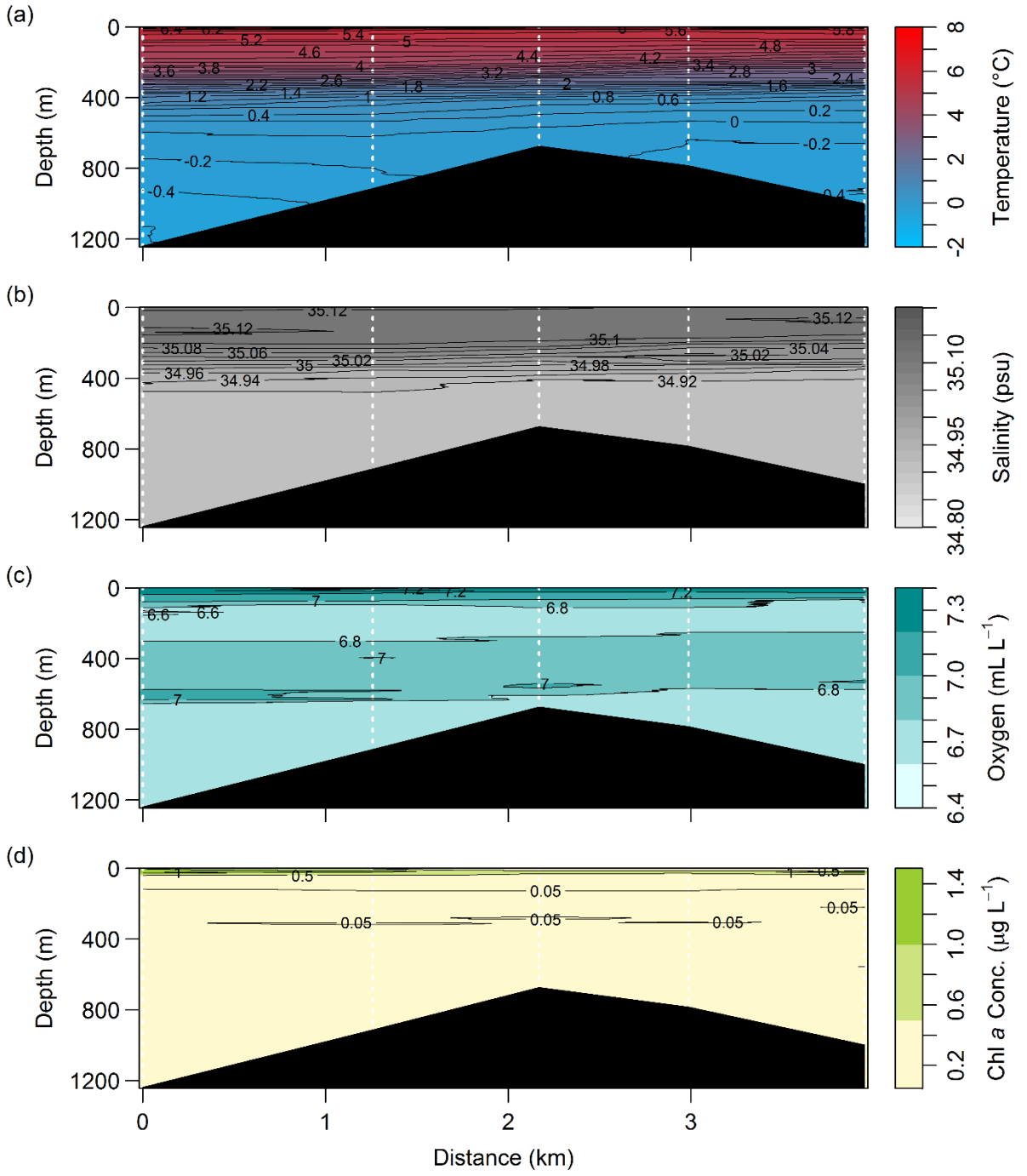

Figure 4 – Cross-sectional distribution of (a) water temperature, (b) salinity, (c) dissolved oxygen concentration, and (d) chlorophyll *a* concentration from the across-ridge water column profiling transect (south-east to north-west).

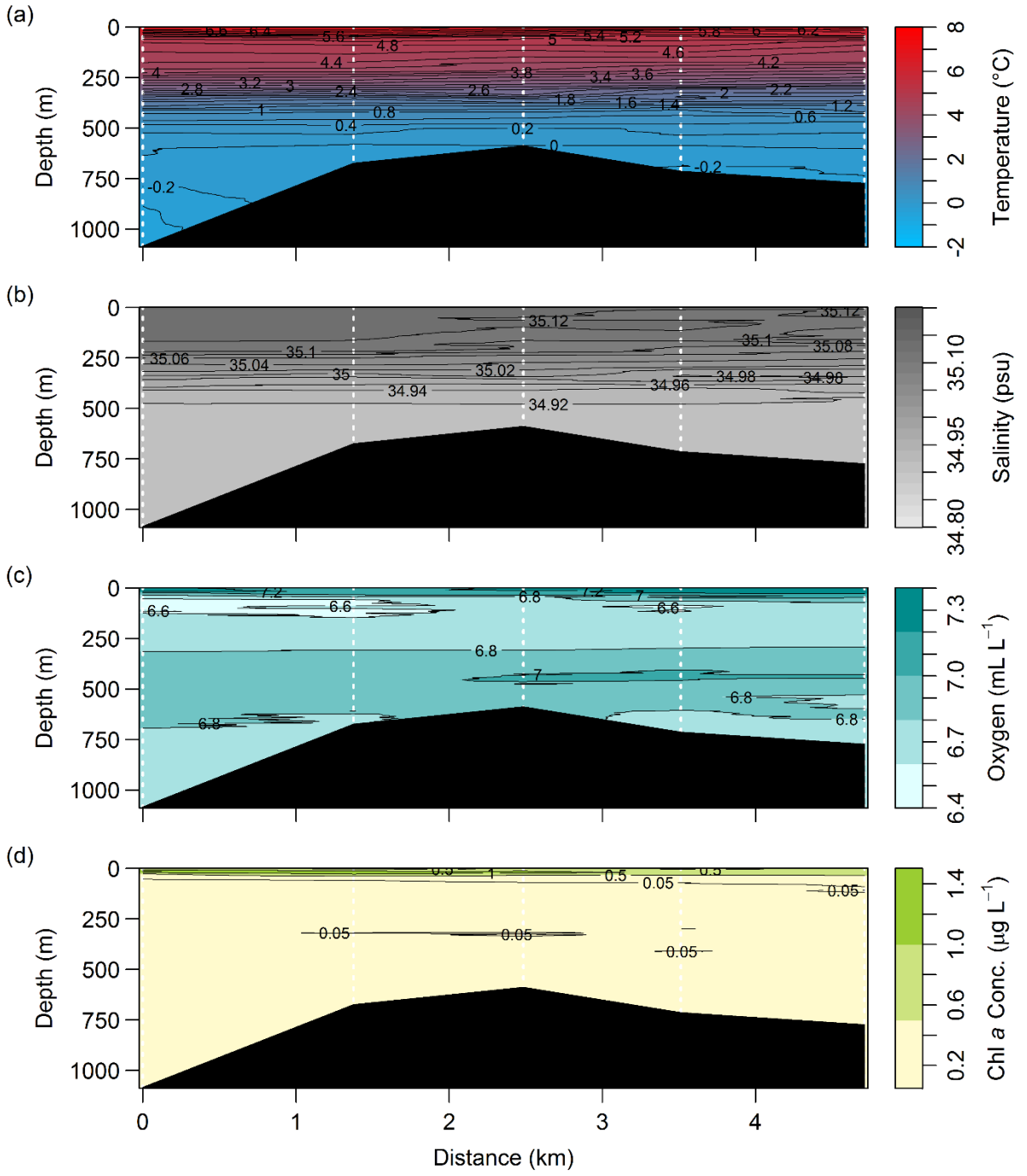

Figure 5 – Cross-sectional distribution of (a) water temperature, (b) salinity, (c) dissolved oxygen concentration, and (d) chlorophyll *a* concentration from the along-ridge water column profiling transect (north-east to south-west).

A potential temperature-salinity (θ-S) diagram was produced (Fig. 6) using all CTD profiles collected in the vicinity of the seamount (i.e., CTD-2 – 11). For each profile, the top 100 m of data were removed because temperature and salinity are influenced by surface processes at these depths (rather than simply the mixing and advection of water masses) and cannot be considered to behave conservatively. The θ-S diagram shows the influence of 3 principal water masses: (1) Norwegian Atlantic Water (NwAtW – θ > 2°C, S > 35 psu); (2) Norwegian Arctic Intermediate Water (NwArIW – θ ≈ 0.5°C, S ≈ 34.88 psu); and (3) Upper Norwegian Deep Water (uNwDW – θ ≈ -0.5°C, S ≈ 34.92 psu) (Hopkins, 1991; Blindheim and Østerhus, 2005). Since NwAtW has its origins in the North Atlantic, North Atlantic Water (NAtW) with θ > 8°C and S > 35.3 psu is its warmest, highest salinity end member (not shown). The coldest end member influencing water mass structure in this region is likely to be Norwegian Deep Water (NwDW - θ ≈ -1.05°C, S ≈ 34.91 psu) (Hopkins, 1991; Blindheim and Østerhus, 2005). The influence of NwArIW occurred at depths corresponding to the oxygen-enriched layer (i.e., between 300 and 600 m).

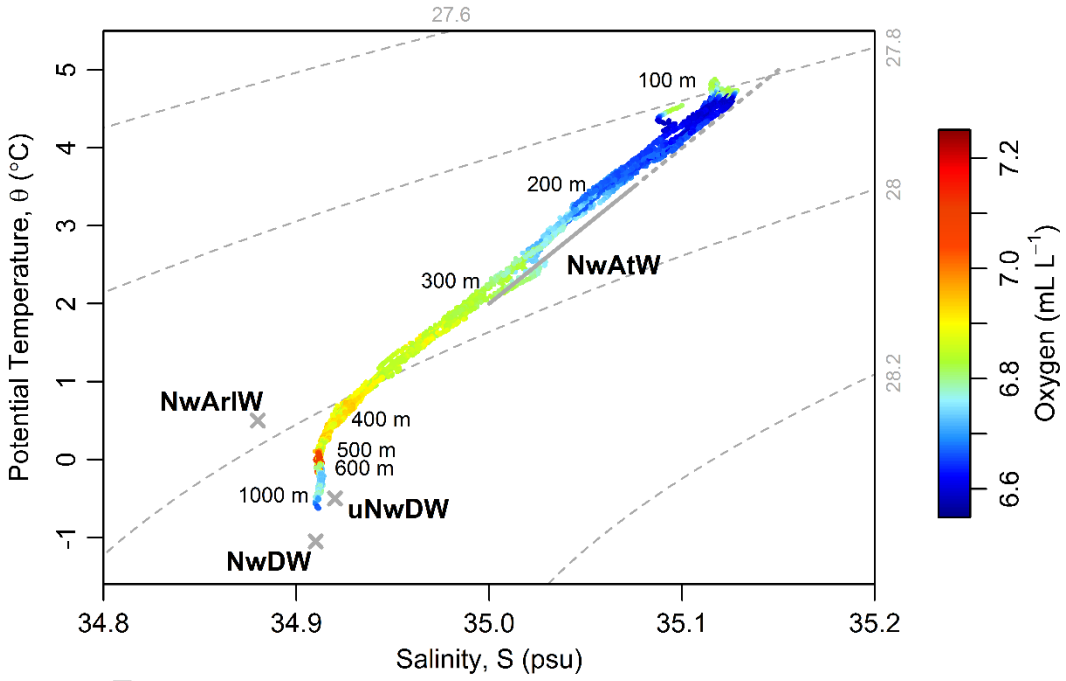

Figure 6 - Potential temperature-salinity (θ-S) diagram showing the water mass structure in the vicinity of the Schultz Massif Seamount (June 2016). Dissolved oxygen concentrations are overlaid. Norwegian Atlantic Water (NwAtW), Norwegian Arctic Intermediate Water (NwArIW), Upper Norwegian Deep Water (uNwDW), and Norwegian Deep Water (NwDW) characteristics are shown using a thick grey line and grey crosses, respectively (values from Hopkins (1991) and Blindheim and Østerhus (2005)). Dashed grey curves are isopycnals (labelled with potential density anomaly, σ_θ, values).

Depth profiles of inorganic nutrient concentrations (PO_4^{3-}, NO_3^- + NO_2^-, Si) and dissolved inorganic carbon (DIC) at SMS are shown in Fig. 7. They combine values from water samples taken during the CTD survey and during ROV dives near the summit. Nutrient concentrations in the surface layer were low, indicating depletion by phytoplankton. They increased, whilst dissolved oxygen decreased, with depth in the surface layer. This likely reflects the combined effects of decreasing phytoplankton photosynthesis, growth, and nutrient uptake with depth and of oxygen depletion and nutrient enhancement by microbial respiration and remineralisation processes near the base of the surface layer. The zone of reduced oxygen concentration at this level (discussed above) is likewise accounted for. Nutrient concentrations and DIC continued to increase with increasing water depth: they were high (relative to surface waters) in the NwArIW (400 – 600 m), and slightly higher still in the uNwDW (> 600 m).

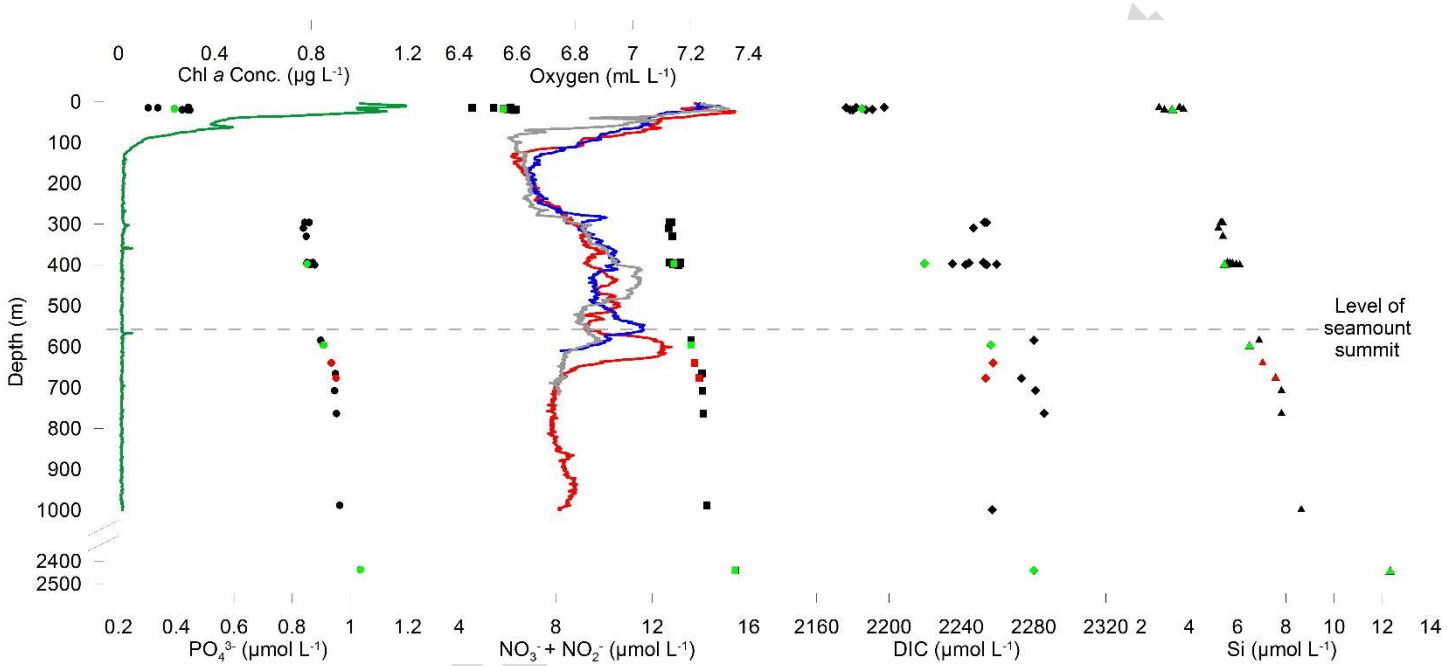

Figure 7 – Vertical profiles of inorganic nutrient concentrations (PO_4^{3-}, NO_3^- + NO_2^-, Si) and dissolved inorganic carbon (DIC) at the Schultz Massif Seamount. Near-seamount values have been combined (black symbols) and are presented with those from opportunistic water sampling during ROV dives to the summit (red points). Values from the deeper, off-seamount reference station (CTD-1) are also included (bright green points). A chlorophyll *a* profile (CTD-2; green line) and several dissolved oxygen profiles (CTD-2, -4, and -10; red, blue, and grey lines, respectively) are plotted to provide context.

Fig. 8 shows depth profiles of SPM at the SMS. All profiles show elevated SPM in the surface layer (~1.5 - 2 mg L^{-1}), likely the result of surface productivity. SPM values were generally smaller at 300 – 400 m water depth (~1 mg L^{-1}), and similar values were observed in deeper waters (at the bottom of profiling casts). An average value for near-bed (0.6 mab) SPM concentration was determined to be 3.2 mg L^{-1} (range: 2.4 – 4.2 mg L^{-1}) using data from the McLane particulate sampler installed on the benthic lander (value shown in Fig. 8 for comparison). Near-bed SPM appeared considerably elevated when compared with values at equivalent depths in adjacent water column profiles. This is indicative of local / near-field particulate resuspension by near-bed currents. Elevated levels of SPM in bottom waters are not clearly detectable in the depth profiles, as the CTD-Rosette unit was rarely permitted to approach the bed to within 10 m.

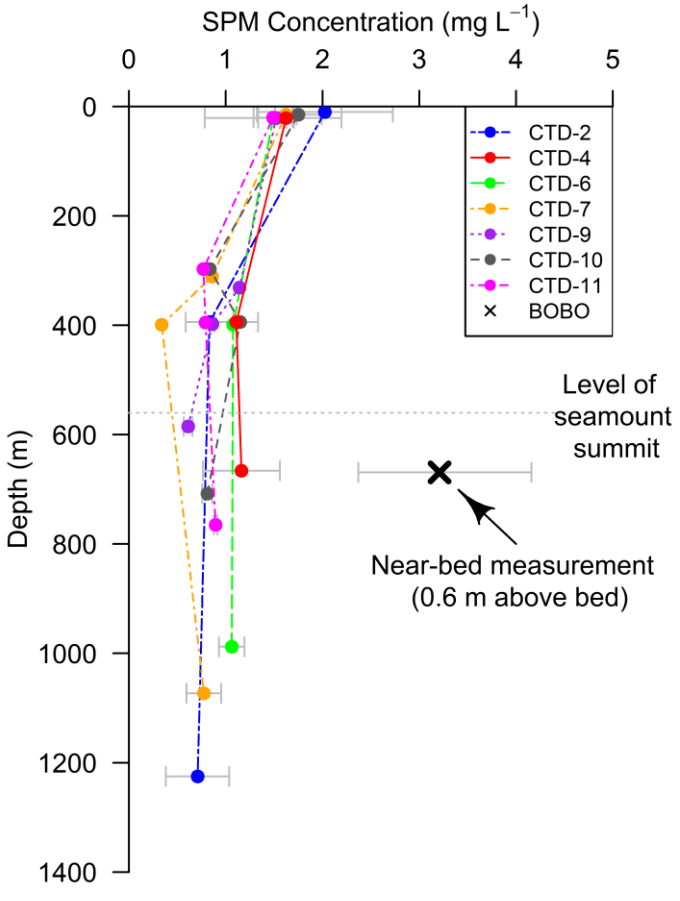

Figure 8 – Vertical profiles of suspended particulate matter (SPM) concentration at the Schultz Massif Seamount. An average near-bed value (i.e., 0.6 mab), determined using data from the benthic lander, is also shown for comparison. Error bars represent the data range for mean-averaged points, and are thus not shown for those depths at which single samples (rather than duplicates) were obtained.

3.3. Near-bed time series data from the benthic lander

Time series data recorded by the BOBO lander are shown in Fig. 9. Regular, in-phase fluctuations were observed in water temperature and dissolved oxygen concentration (Fig. 9 (a) and (b)). Each consisted of (1) a 'jump-relax' event (shaded grey in Fig. 9) characterised by an initial step-increase and a gradual decline (exhibiting a secondary, less pronounced local maximum) and (2) a short period of lower temperature and dissolved oxygen (typically exhibiting reduced temporal variability in both parameters). For the two entire cycles captured in the record, the period was 25.7 and 26.7 h (measured from step-increase to step-increase). Further (partial) cycles can be discerned at the start and end of the record.

The temperature and dissolved oxygen signals had a fixed-phase relationship with periodic variations in near-bed suspended particle speeds and particularly directions (Fig. 9 (c) and (d)), as determined from video analysis. Change of particle direction coincided with the step-increases in temperature and dissolved oxygen, and the particles continued in that direction (left to right, laterally in the benthic boundary layer) during the gradual relaxation of these parameters. Particle direction reversed (right to left) for the duration of the short 'reduced-variability' stages, with the result that the periodic variations in particle direction were somewhat asymmetric (particles travelled for longer in one direction than in the reverse). Particle speeds were generally elevated during the longer 'jump-relax' stage, exhibiting two peaks during these periods. They were typically lower during the shorter 'reduced-variability' stage. The data derived from lander video analysis in this paper are subject to several limitations (see *Materials and methods*) but offer qualitative insight. Taking particle speed and direction as proxies for current speed and direction, the fixed-phase relationship with temperature and dissolved oxygen suggests a hydrodynamical phenomenon is responsible for the temporal behaviour of these parameters. Diurnal tidal forcing is likely important, given the periods between successive 'jumps' and the periodicity of the particle direction behaviour, but this does not preclude the influence of higher frequency signals. For example, the secondary local maxima in temperature and dissolved oxygen (i.e., those peaks that are not 'jump'-like), and associated peaks in particle speed, occurring throughout the record could indicate the influence of shorter period tidal constituents or inertial motions.

To support near-bed flow information inferred from video analysis, data were extracted from a regional barotropic inverse tidal solution using the Oregon State University Tidal Inversion Software (OTIS – 'Iceland' domain; Egbert and Erofeeva, 2002). Harmonic constants for key tidal constituents at the SMS are shown in Table S1, and tidal current amplitudes indicate that diurnal constituents are

indeed likely to dominate the local velocity field. In fact, the importance of the luni-solar diurnal tidal constituent (K_1) relative to the principal lunar semi-diurnal constituent (M_2) appears to increase in the vicinity of the SMS (Fig. S3). Tidal current predictions from OTIS for the SMS at the time of the lander observations show encouragingly similar patterns to those in the dataset inferred from analysis of the lander video (see Fig. S4(b-d)), including strong asymmetry in the current direction signal (Fig. S4(d)). Predicted current speeds from OTIS appear too low, however, being almost 3 cm s^{-1} at peak flow. The limitations of the particle motion analysis (section 2.3) have prevented presentation of flow information in such regular units in this article. However, based on features visible in the video footage, estimated peak flow speeds are of the order of 25 cm s^{-1} for this window of observation, and are indicative of enhanced flows at the SMS summit.

The temperatures immediately before and after the largest 'jump' in the lander record were extracted (-0.21°C and -0.05°C, respectively) and compared to adjacent CTD profiles, in order to determine the depths at which waters of these temperatures typically occur and their vertical separation. These two values were separated by 131 ± 50 m water depth (mean ± SD), averaged across 4 CTD profiles from the nearest stations adjacent to the lander's position (i.e., CTD-3, -5, -10, -11). The cast at CTD-4, nearest the lander site, was not deep enough to capture the full range of temperatures experienced by the lander, and so could not be used for this purpose. This analysis suggests that vertical displacements of water / isotherms by 130 m or more can occur at this location, interacting with the seamount summit with a periodicity of slightly longer than 1 d. The warmest water incident upon the lander site (669 m water depth) was more typically found 72 m higher in the water column (at 597 ± 40 m depth (mean ± SD)), at the base of the layer of NwArIW. The change in water temperature at the time of a 'jump' is fairly rapid, occurring in 15 min or less.

Note that a decreasing trend was apparent in the dissolved oxygen record but, owing to the short duration of the time series, it is unclear whether this can be attributed to longer timescale variability or to gradual acclimatisation of the instrument to a deep-sea environment. The salinity record has been omitted from Fig. 9 because fluctuations in salinity were small to negligible and no clear temporal pattern could be discerned above noise (i.e., short periods of spikey salinity data at step-changes in temperature, most likely the result of thermal-lag induced instrumental error – see Garau et al. (2011)). De-spiking and interpolation of the salinity record could not be achieved with sufficient scientific rigour, but visual inspection confirmed an estimated mean salinity value of 34.91 psu is appropriate. This is consistent with values at the same water depth from the CTD survey.

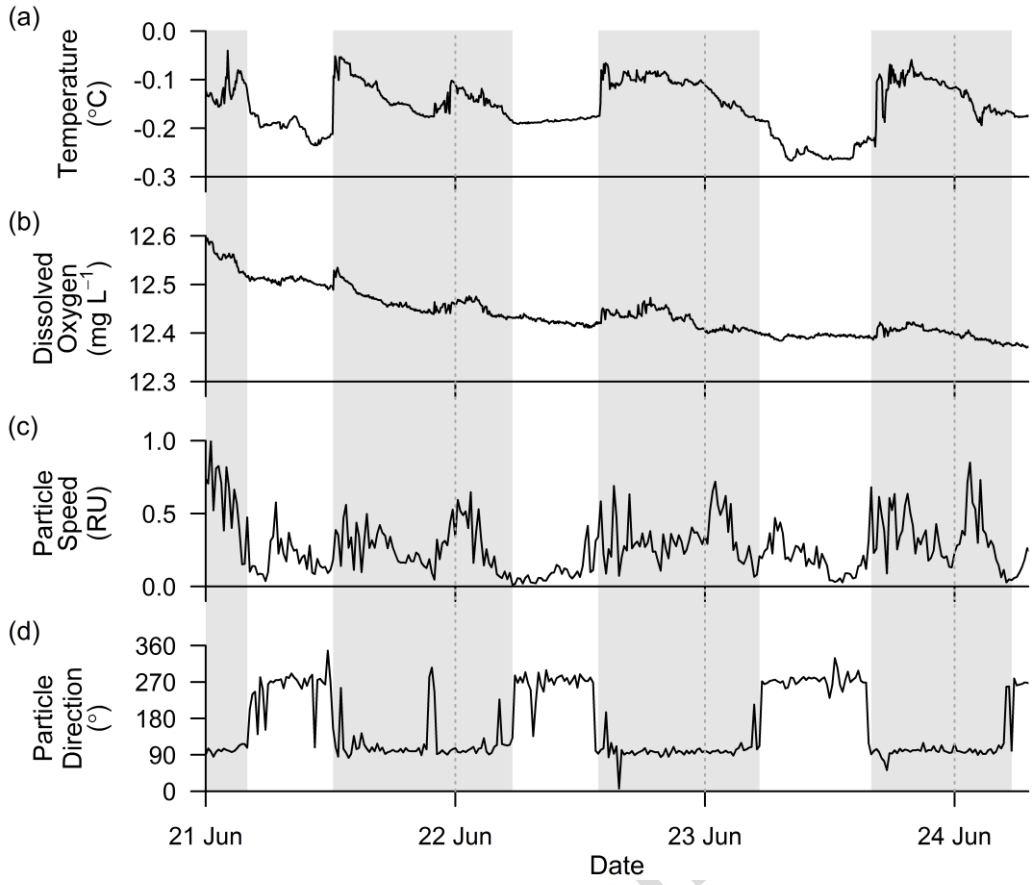

Figure 9 - Time series data from the Bottom Boundary (BOBO) Benthic Lander deployed near the seamount summit for c. 3 days in June 2016. Panels show (a) water temperature, (b) dissolved oxygen concentration, (c) suspended particle speed, and (d) suspended particle direction (0°=up (in the video footage); 180°=down; 90°=towards the right; 270°=towards the left; see *Materials and methods*). Grey-shaded areas highlight 'jump-relax' events in temperature and dissolved oxygen and associated features in particle speed and direction (see text).

4. Discussion

The purpose of this study was to characterise the oceanographic setting and short-timescale environmental variability at the SMS in order to identify environmental conditions that sustain and influence a dense sponge ground on its summit. The summit coincided approximately with the lower boundary of an intermediate water mass, believed to be Norwegian Arctic Intermediate Water (NwArIW) (Blindheim, 1990; Hopkins, 1991; Blindheim and Rey, 2000; Jeansson et al., 2017). This had a slightly higher temperature and dissolved oxygen concentration than the deep water mass below (Upper Norwegian Deep Water – uNwDW), to which the seamount flanks were exposed. Time series records from a site just below the seamount summit revealed a series of regular fluctuations in water temperature and dissolved oxygen concentration. These events corresponded with patterns in reversing near-bed currents, which had a periodicity approximately equal to that of the diurnal tide. Comparison of maximum and minimum temperatures from the time series with temperature profiles from the CTD survey suggests that the fluctuations represent periodic impingement of waters upon the summit that are typically separated by around 130 m depth in the adjacent water column. The warmest water incident upon the lander was typically found 72 m higher in the water column, at the base of the layer of NwArIW. It appears that the summit of the SMS hosts a dynamic environment that is predominantly tidally-forced, a feature common to several sponge-dominated communities described in the scientific literature (see section 4.2. – *Biological response*).

Other potentially important factors were observed, and are summarised here. Near-bed SPM levels were elevated compared to those in the adjacent water column. Particulate matter was transported laterally in the benthic boundary layer. Its direction of travel underwent frequent reversal, and transport was asymmetric (discussed below). Lenses of water with enhanced chlorophyll *a* concentration were apparent above the seamount summit (at the base of the permanent thermocline / top of the layer of NwArIW). Levels of inorganic nutrients and DIC in uNwDW were slightly elevated compared to NwArIW. Horizontal gradients of salinity and dissolved oxygen concentration were observed at shallow depths during the along-ridge CTD transect (Fig. 5(b) and (c)), possibly indicating the proximity of a front between surface water masses.

Two main questions arise, which are addressed below. What is the dynamical phenomenon responsible for the observed temporal variability in near-bed parameters? How is the observed environmental setting likely to influence sponges on the summit?

4.1. Hydrodynamics

It has not been possible to fully describe the prevailing hydrodynamics at the SMS summit on the basis of a short-term current record, from a single site, containing derived (rather than directly measured) information (see section 2.3.). However, diurnal tidal forcing appears important. The amplification of diurnal tidal currents at seamount summits and other isolated topographic features is regularly reported in the scientific literature (e.g., Eriksen, 1991; Haidvogel et al., 1993 (and references therein); Brink, 1995; Codiga and Eriksen, 1997). Exactly how seamounts intensify such currents is yet to be clearly established (Kunze and Toole, 1997).

Reflection of incident internal waves has been proposed as one explanatory mechanism (Kunze and Sanford, 1986). The SMS site (latitude: 73° 47'N) is above the critical 'diurnal turning' latitude (~30°N and S) at which the diurnal tidal frequency equals the inertial frequency. Below this critical latitude, diurnal period internal waves are superinertial and can propagate freely (Kunze and Sanford, 1986; Kulikov et al., 2010). Above it, they are subinertial and cannot do so (Kunze and Sanford, 1986; Kulikov et al., 2010). It is therefore unlikely that diurnal period internal waves from remote sources could be incident upon (and reflected from) the seamount, intensifying near-bed currents. The SMS is <1° of latitude below a critical 'semi-diurnal turning' latitude (~74.5°N and S for the principal lunar semi-diurnal tidal constituent (M_2)). Semi-diurnal period internal waves are superinertial at the latitude of the SMS and can propagate freely. Thus, incoming semi-diurnal internal waves may potentially contribute to bottom current amplification at the SMS. Although a diurnal signal clearly dominates the timeseries record from the benthic lander, there is some evidence to suggest fluctuations of a higher (possibly semi-diurnal/inertial) frequency. Contribution from the semi-diurnal tide is not unexpected at the latitude of the SMS through mechanisms other than reflection of internal waves. Indeed, several authors have found internal tidal currents to be significantly amplified at near-critical latitudes (such as we have here for the M_2 tide) (Munk and Phillips, 1968; Furevik and Foldvik, 1996; Kulikov et al., 2010).

Baroclinic wave motions that are trapped to seamount topography ('seamount-trapped' topographic waves) are often cited as a mechanism by which oscillating bottom currents may be amplified (Chapman, 1989; Eriksen, 1991; Haidvogel et al., 1993; Brink, 1995; Codiga and Eriksen, 1997). These are believed to be resonantly generated and excited to substantial amplitudes by relatively weak oscillatory flows (e.g., the diurnal tide in many parts of the deep open ocean) (Chapman, 1989; Brink, 1990; Eriksen, 1991; Haidvogel et al., 1993). Internal wave motion generated locally may also persist as 'vortex-trapped' waves (i.e., trapped in circulation patterns existing around the seamount

summit) (Kunze and Toole, 1997; White et al., 2007). In both cases, diurnal tidal motions are likely to feature more prominently because the site is above the critical 'diurnal turning' latitude, rendering such motions unable to propagate away freely. Vortex-trapped diurnal internal waves are subject to constraints of scale above about 40°N and S (see Kunze and Toole, 1997), and so seamount-trapped topographic waves of diurnal periodicity may be more likely at the SMS.

The current record obtained in this work suggests asymmetry in tidal transport (i.e., the current flows faster and for longer duration in one direction than in the reverse). Tidal rectification, resulting from non-linear interaction between enhanced tidal currents and steep bathymetry, is a potential explanatory mechanism and one that has been reported for seamounts (Eriksen, 1991; Brink, 1995; White et al., 2007). Asymmetry is also present in the OTIS (barotropic) tidal current predictions for the SMS during the observation period (Fig. S4). The temperature and dissolved oxygen fluctuations in the time series data may be caused either directly by vertical motions associated with seamount-trapped topographic waves (Kunze and Toole, 1997) or as a local consequence of an enhanced tide. In the latter case, topographic acceleration of tidal currents passing over, for example, the strong ridges either side of the lander site may hydraulically generate transient downwelling 'events' downstream of the topographic feature (Davies et al., 2009). This has been shown to influence food supply to other communities of suspension feeders (Davies et al., 2009).

Lenses of water with elevated chlorophyll *a* concentration and turbidity occurring directly above the summit of a seamount, as observed in this study, have been associated with the retention of passive particles by anti-cyclonic (in the Northern Hemisphere) horizontal circulation around the summit and associated secondary circulation in the vertical-radial plane (Goldner and Chapman, 1997; Beckmann and Mohn, 2002). Whilst the existence of such circulation cells at the SMS cannot be confirmed on the basis of this study, tidal rectification (discussed above) has also been implicated in driving horizontal circulation at other seamounts (Eriksen, 1991; Brink, 1995; Kunze and Toole, 1997).

Classically, mean circulation patterns over seamounts have been attributed to steady impinging flows (rather than rectified tidal currents), and are explained in terms of Taylor-Proudman dynamics (based on vorticity arguments) (Proudman, 1916; Taylor, 1917). Jet currents, topographically-steered by the AMOR, are thought to exist at depth in the region (Orvik and Niiler, 2002), and could provide the flow required to generate a so-called 'Taylor cap' above the SMS. A Taylor cap is an isolated anti-cyclonic (in the Northern Hemisphere) flow pattern about a seamount.

The ability of the SMS to host a Taylor cap can be explored by calculating three non-dimensional parameters that characterise the flow, stratification, and seamount height: the Rossby number, $R_o = U/fL$ (representing the ratio of advective to rotational effects); the Burger number, $S = NH/fL$ (a measure of the importance of the stratification relative to rotational effects); and the fractional seamount height, $\delta = h_m/H$. In these equations, U is a steady inflow velocity, f the Coriolis frequency, L the seamount horizontal length scale, N the Brunt-Väisälä buoyancy frequency, H the water depth (in the absence of the seamount), and h_m the height of the seamount above the bottom. Given the situation of the SMS on a mid-ocean ridge system, estimating its horizontal extent is difficult. We employ L = 7 km, based on the bathymetry shown in Fig. 1(b) and determined as the average of the major and minor axes of the elliptical seamount footprint (10 km and 4 km, respectively). This represents the lower bound of possible estimates. At the latitude of the SMS, $f = 1.4 \times 10^{-4}$ rad s^{-1}, and the product fL is conveniently close to unity, giving Rossby numbers of 0.05 - 0.3 for flows (U) of 5 – 30 cm s^{-1}. The fractional height, δ, of the SMS is sensitive to the values selected for H and h_m, but a range of approaches returns values between 0.6 and 0.8. Selecting an appropriate value for H is also difficult for a seamount rising from a ridge system already elevated relative to adjacent basins. In the discussion that follows, we use H = 1400 m and h_m = 837 m (i.e., δ = 0.6) for consistency with our estimate of L taken from Fig. 1(b), but larger values could also be considered appropriate. By comparison with the work of Chapman and Haidvogel (1992) (see Fig. 20 in that work), our calculated Rossby numbers span a critical threshold delineating the occurrence (low R_o) and non-occurrence (high R_o) of Taylor caps for seamounts in this height range.

It would appear that the SMS could host a Taylor cap, or what Chapman and Haidvogel (1992) refer to as temporary trapping (a transient cap), under weak, steady flow conditions. A representative length scale, L, for the SMS may be larger than that estimated above. In such a case, smaller R_o values would be returned for the same range of inflow currents, further favouring the possible occurrence of a Taylor cap. The numerical model outputs of Chapman and Haidvogel (1992) were for steady, stratified impinging flows with Burger number S = 1, whereas here S is greater (~1.4; calculated using a representative N value from below the permanent pycnocline of 9.6×10^{-4} rad s^{-1}). This will have implications for the critical Rossby number separating the occurrence and non-occurrence of Taylor caps, but is unlikely to alter the broader interpretation that Taylor caps are theoretically possible at the SMS under weak flows. The models were run with the simplifying assumptions of an isolated, smooth, axisymmetric seamount topography and a non-periodic flow regime, which do not hold at the SMS with potential implications for Taylor cap development.

Evidence of the clear isopycnal doming that is expected in association with vortex caps (either Taylor caps or those generated by tidal rectification) over seamounts is not compelling at the SMS (Figs. 4 and 5). Calculating the decay height (H_d) of a hypothetical Taylor cap at the SMS, using the equation fL/N of Brechner Owens and Hogg (1980), gives H_d = 1021 m for f, L, and N values as stated above. This suggests that, under steady flow, the SMS could cause local mesoscale variability up to at most ~200 m above its summit (i.e., up to the base of the permanent pycnocline). The vertical extent of its influence is likely to be smaller still because it will be truncated further by the higher levels of stratification present above the seamount. This may explain the absence of clear isopycnal doming in the CTD transect data. A hydrographic survey designed to measure currents at various positions on the seamount, quantify the strength and nature of any mean circulation, and determine the relative importance of tidal and steady-flow dynamics would be revealing in this respect.

4.2. Biological response

Sponges living on the SMS summit are likely to benefit from several of the observed factors identified above. The seamount is deep (*sensu* Pitcher et al. (2007)) and situated within very cold waters (i.e., <0°C). The summit is periodically flushed with slightly warmer, oxygen-enriched water from the core of Norwegian Arctic Intermediate Water (NwArIW) above, which may boost metabolic processes. Its location at the boundary of two water masses may ensure that the summit sponge ground also benefits from the slightly elevated inorganic nutrient and DIC concentrations of the Upper Norwegian Deep Water (uNwDW) below, supplied through the turbulence and mixing generated by the hydrodynamical processes discussed. Near-bed SPM concentrations are elevated compared with the adjacent water column (probably through local / near-field resuspension by tidal currents), improving food supply to the sponges. Particulates are advected laterally in the benthic boundary layer by oscillating, temporally asymmetric tidal currents, which increase particle residency times near the sponges, whilst also supplying 'fresh' particles and acting to prevent smothering by sedimentation. Furthermore, any retention of passive organic material above the seamount (i.e., the lenses of elevated chl *a* and turbidity) has implications for food supply and recruitment.

The summit of the SMS is assumed to have provided suitable substrate for the initial growth of sponges and, since then, a spicule mat (~10 - 20 cm thick - data not presented in this article) has developed at the sediment interface, supporting the existence of the sponge ground in the present day. Appropriate substrate availability is a key abiotic factor driving the spatial distribution of sponges (Barthel and Gutt, 1992; Barthel and Tendal, 1993). Investigations that aim to establish the

relative importance of different factors to sponge distribution are recommended. These could take the form of correlating changes in sponge density and diversity with depth against changes not only in the oceanographic factors identified in this work but also in other important factors, such as surficial geology and biotic interactions.

Our findings and interpretations are consistent with those of several other authors. Whitney et al. (2005) attributed the persistence of hexactinellid sponge reefs at the heads of shelf canyons to several factors, including the presence of nutrient rich waters, the supply of SPM, and the local prevalence of tidally-modulated near-bed currents that increase particle residency times and prevent smothering of the sponges. Genin et al. (1986), Rice et al. (1990), and White (2003) all highlighted a potential link between enhanced near-bed currents, improved food supply (and/or larval recruit supply, in the case of Genin et al. (1986)), and the occurrence of sponge-dominated communities. Klitgaard and Tendal (2004) discussed the detrimental (smothering) effect of high suspended particulate loads that settle out, which by extension highlights the value to sponge grounds of a current regime that prevents this from occurring. Beazley et al. (2015) concluded that the presence of dense sponge grounds could potentially be attributed to a warmer water mass residing in their study area. Several other authors have related the presence of sponges to that of a specific water mass in the study region (Barthel et al., 1996; Klitgaard and Tendal, 2004; Murillo et al., 2012). Finally, White et al. (2007) noted that the retention of suspended organic material over seamounts could indicate enclosed circulation patterns, which sometimes include a downwelling component likely to be important to benthic organisms located there.

The results presented here identify a subtle interplay between the hydrodynamics of the seamount summit and the water masses located above and below, which may be an important factor in explaining the success of the dense sponge ground occupying the summit. Time series measurements came from a benthic lander positioned 70 - 80 m below the true summit. Given that the most energetic water motions associated with seamounts are typically concentrated near the very top (Brink, 1989; Chapman, 1989), it is possible that several of the beneficial factors discussed above are further enhanced there.

4.3. Conclusion

Interaction between seamount geomorphology, hydrodynamic regime, and water column structure resulted in several environmental factors that may benefit sponges and help explain enhanced sponge density and diversity at the summit of the SMS. The sponge ground occurred within nutrient-

rich waters (NwArIW / uNwDW boundary). It was regularly flushed with warmer, oxygen-enriched water from above (NwArIW). It was also exposed to elevated near-bed SPM levels, and experienced favourable (diurnal tidal) currents that potentially enhance food supply and prevent smothering by sedimentation. Elevated chlorophyll *a* concentration observed in the mid-water column above the summit may indicate passive particle retention by seamount-scale circulation patterns with further implications for food supply and recruitment.

The primary limitation of the work was that the hydrodynamical setting could not be characterised fully on a summit-wide scale. Furthermore, the observed hydrodynamics may not persist throughout the year, represent the dominant phenomena over longer time scales, or reflect those most important to the sponges. Several longer-term moorings would be required to resolve these questions. Owing to the global diversity in seamount morphology and oceanographic setting, the results of this study cannot be generalised to all seamounts. However, it is likely that they may be generalisable to similar seamounts known to exist along the AMOR. The broad implication is that, if dense seamount sponge grounds (such as that at the SMS) and their associated ecosystems are sustained by the coincidence of multiple beneficial environmental factors acting in synergy at a given location / depth, they may be sensitive to changes across a particularly broad range of abiotic factors (e.g., under climate change, or anthropogenic activities in the deep sea).

Acknowledgements

This research has been performed in the scope of the SponGES project, which received funding from the European Union's Horizon 2020 research and innovation programme under grant agreement No. 679849. This document reflects only the authors' views and the Executive Agency for Small and Medium-sized Enterprises (EASME) is not responsible for any use that may be made of the information it contains. Furu Mienis is supported financially by the Innovational Research Incentives Scheme of the Netherlands Organisation for Scientific Research (NWO-VIDI). A Nuffield research placement scheme supported Bryn Harris, who is thanked for undertaking the lander video analysis. The University of Bergen is thanked for providing ship time for the project. The authors are indebted to Bob Koster and Bernt Olsen, and to the captain and crew of *RV G.O. Sars*. Malen Roberts, David Bowers, and Susan Allender are thanked for their comments on the manuscript.

Data availability statement

Datasets presented in this article are available at https://doi.org/10.1594/PANGAEA.891035

Conflicts of interest

None to declare.

References

Amsler, M. O., McClintock, J. B., Amsler, C. D., Angus, R. A., & Baker, B. J. (2009). An evaluation of sponge-associated amphipods from the Antarctic Peninsula. *Antarctic Science*, *21*(6), 579–589. https://doi.org/10.1017/S0954102009990356

Barthel, D. (1992). Do hexactinellids structure antarctic sponge associations? *Ophelia*, *36*(2), 111–118.

Barthel, D., & Gutt, J. (1992). Sponge associations in the eastern Weddell Sea. *Antarctic Science*, *4*(2), 137-150. https://doi.org/10.1017/S0954102092000221

Barthel, D., & Tendal, O. S. (1993). The sponge association of the abyssal Norwegian-Greenland Sea: Species composition, substrate relationships, and distribution. *Sarsia*, *78*(2), 83–96.

Barthel, D., Tendal, O. S., & Thiel, H. (1996). A wandering population of the hexactinellid sponge *Pheronema carpenteri* on the continental slope off Morocco, Northwest Africa. *Marine Ecology*, *17*(4), 603–616. https://doi.org/10.1111/j.1439-0485.1996.tb00420.x

Beazley, L. I., Kenchington, E. L., Murillo, F. J., & Sacau, M. (2013). Deep-sea sponge grounds enhance diversity and abundance of epibenthic megafauna in the Northwest Atlantic. *ICES Journal of Marine Science*, *70*, 1471–1490. https://doi.org/10.1093/icesjms/fst124

Beazley, L., Kenchington, E., Yashayaev, I., & Murillo, F. J. (2015). Drivers of epibenthic megafaunal composition in the sponge grounds of the Sackville Spur, Northwest Atlantic. *Deep-Sea Research Part I: Oceanographic Research Papers*, *98*, 102–114. https://doi.org/10.1016/j.dsr.2014.11.016

Beckmann, A., & Mohn, C. (2002). The upper ocean circulation at Great Meteor Seamount. Part II: Retention potential of the seamount induced circulation. *Ocean Dynamics*, *52*(4), 194–204.

Belarbi, E. H., Contreras Gómez, A., Chisti, Y., García Camacho, F., & Molina Grima, E. (2003). Producing drugs from marine sponges. *Biotechnology Advances*, *21*(7), 585–598. https://doi.org/10.1016/S0734-9750(03)00100-9

Bell, J. J. (2008). The functional roles of marine sponges. *Estuarine, Coastal and Shelf Science*, *79*(3), 341–353. https://doi.org/10.1016/j.ecss.2008.05.002

Bett, B. J., & Rice, A. L. (1992). The influence of hexactinellid sponge (*Pheronema carpenteri*) spicules on the patchy distribution of macrobenthos in the Porcupine Seabight (bathyal NE Atlantic). *Ophelia*, *36*(3), 217–226. https://doi.org/10.1080/00785326.1992.10430372

Blindheim, J. (1990). Arctic Intermediate Water in the Norwegian sea. *Deep Sea Research Part A, Oceanographic Research Papers*, *37*(9), 1475–1489. https://doi.org/10.1016/0198-0149(90)90138-L

Blindheim, J., & Østerhus, S. (2005). The Nordic Seas, main oceanographic features. In H. Drange, T.

Dokken, T. Furevik, R. Gerdes, & W. Berger (Eds.), *The Nordic Seas: An Integrated Perspective* (pp. 11–37). Washington DC: American Geophysical Union. https://doi.org/10.1029/158GM03

Blindheim, J., & Rey, F. (2004). Water-mass formation and distribution in the Nordic Seas during the 1990s. *ICES Journal of Marine Science*, *61*(5), 846–863. https://doi.org/10.1016/j.icesjms.2004.05.003

Bo, M., Bertolino, M., Bavestrello, G., Canese, S., Giusti, M., Angiolillo, M., … Taviani, M. (2012). Role of deep sponge grounds in the Mediterranean Sea: A case study in southern Italy. *Hydrobiologia*, *687*(1), 163–177. https://doi.org/10.1007/s10750-011-0964-1

Brechner Owens, W., & Hogg, N. G. (1980). Oceanic observations of stratified Taylor columns near a bump. *Deep Sea Research Part A, Oceanographic Research Papers*, *27*(12), 1029–1045. https://doi.org/10.1016/0198-0149(80)90063-1

Brink, K. H. (1989). The effect of stratification on seamount-trapped waves. *Deep Sea Research Part A, Oceanographic Research Papers*, *36*(6), 825–844. https://doi.org/10.1016/0198-0149(89)90031-9

Brink, K. H. (1990). On the generation of seamount-trapped waves. *Deep Sea Research Part A, Oceanographic Research Papers*, *37*(10), 1569–1582. https://doi.org/10.1016/0198-0149(90)90062-Z

Brink, K. H. (1995). Tidal and lower frequency currents above Fieberling Guyot. *J. Geophys. Res.*, *100*(C6), 10,817-10,832.

Bruvoll, V., Breivik, A. J., Mjelde, R., & Pedersen, R. B. (2009). Burial of the Mohn-Knipovich seafloor spreading ridge by the Bear Island Fan: Time constraints on tectonic evolution from seismic stratigraphy. *Tectonics*, *28*(4), 1–14. https://doi.org/10.1029/2008TC002396

Buhl-Mortensen, L., Vanreusel, A., Gooday, A. J., Levin, L. A., Priede, I. G., Buhl-Mortensen, P., … Raes, M. (2010). Biological structures as a source of habitat heterogeneity and biodiversity on the deep ocean margins. *Marine Ecology*, *31*(1), 21–50. https://doi.org/10.1111/j.1439-0485.2010.00359.x

Cárdenas, P., Rapp, H. T., Klitgaard, A. B., Best, M., Thollesson, M., & Tendal, O. S. (2013). Taxonomy, biogeography and DNA barcodes of *Geodia* species (Porifera, Demospongiae, Tetractinellida) in the Atlantic boreo-arctic region. *Zoological Journal of the Linnean Society*, *169*(2), 251–311. https://doi.org/10.1111/zoj.12056

Carmack, E., & Aagaard, K. (1973). On the deep water of the Greenland Sea. *Deep-Sea Research*, *20*(8), 687–715. https://doi.org/10.1016/0011-7471(73)90086-7

Cathalot, C., Van Oevelen, D., Cox, T. J. S., Kutti, T., Lavaleye, M., Duineveld, G., & Meysman, F. J. R. (2015). Cold-water coral reefs and adjacent sponge grounds: hotspots of benthic respiration

and organic carbon cycling in the deep sea. *Frontiers in Marine Science*, *2*(June), 1–12. https://doi.org/10.3389/fmars.2015.00037

Chapman, D. C. (1989). Enhanced subinertial diurnal tides over isolated topographic features. *Deep Sea Research Part A, Oceanographic Research Papers*, *36*(6), 815–824. https://doi.org/10.1016/0198-0149(89)90030-7

Chapman, D. C., & Haidvogel, D. B. (1992). Formation of Taylor caps over a tall isolated seamount in a stratified ocean. *Geophysical & Astrophysical Fluid Dynamics, 64*(1-4), 31-65. https://doi.org/10.1080/03091929208228084

Codiga, D. L., & Eriksen, C. C. (1997). Observations of low-frequency circulation and amplified subinertial tidal currents at Cobb Seamount. *J. Geophys. Res.*, *102*(C10), 22,993-23,007.

Davies, A. J., Duineveld, G. C. A., Lavaleye, M. S. S., Bergman, M. J. N., van Haren, H., & Roberts, J. M. (2009). Downwelling and deep-water bottom currents as food supply mechanisms to the cold-water coral *Lophelia pertusa* (Scleractinia) at the Mingulay Reef complex. *Limnology and Oceanography*, *54*(2), 620–629. https://doi.org/10.4319/lo.2009.54.2.0620

Davies, A. J., Duineveld, G. C. A., van Weering, T. C. E., Mienis, F., Quattrini, A. M., Seim, H. E., … Ross, S. W. (2010). Short-term environmental variability in cold-water coral habitat at Viosca Knoll, Gulf of Mexico. *Deep-Sea Research Part I: Oceanographic Research Papers*, *57*(2), 199–212. https://doi.org/10.1016/j.dsr.2009.10.012

De Goeij, J. M., Van Oevelen, D., Vermeij, M. J. A., Osinga, R., Middelburg, J. J., De Goeij, A. F. P. M., & Admiraal, W. (2013). Surviving in a marine desert: The sponge loop retains resources within coral reefs. *Science*, *342*(October), 108–110. https://doi.org/10.1126/science.1241981

Dickson, R. R., & Brown, J. (1994). The production of North Atlantic Deep Water: Sources, rates, and pathways. *J. Geophys. Res.*, *99*(C6), 12,319-12,341.

Dudik, O., Leonor, I., Xavier, J. R., Rapp, H. T., Pires, R. A., Silva, T. H., & Reis, R. L. (2018). Sponge-derived silica for tissue regeneration: Bioceramics of deep-sea sponge. *Materials Today*. https://doi.org/10.1016/j.mattod.2018.03.025

Durán Muñoz, P., Murillo, F. J., Sayago-Gil, M., Serrano, A., Laporta, M., Otero, I., & Gómez, C. (2011). Effects of deep-sea bottom longlining on the Hatton Bank fish communities and benthic ecosystem, north-east Atlantic. *Journal of the Marine Biological Association of the United Kingdom*, *91*(4), 939–952. https://doi.org/10.1017/S0025315410001773

Egbert, G. D., & Erofeeva, S. Y. (2002). Efficient Inverse Modeling of Barotropic Ocean Tides. *Journal of Atmospheric and Oceanic Technology*, *19*(2), 183-204. https://doi.org/10.1175/1520-0426(2002)019<0183:EIMOBO>2.0.CO;2

Ehrlich, H., Steck, E., Ilan, M., Maldonado, M., Muricy, G., Bavestrello, G., … Richter, W. (2010).

Three-dimensional chitin-based scaffolds from Verongida sponges (Demospongiae: Porifera). Part II: Biomimetic potential and applications. *International Journal of Biological Macromolecules*, *47*(2), 141–145. https://doi.org/10.1016/j.ijbiomac.2010.05.009

Eriksen, C. C. (1991). Observations of amplified flows atop a large seamount. *J. Geophys. Res.*, *96*(C8), 15,227-15,236.

FAO. (2009). *International guidelines for the management of deep-sea fisheries in the high seas*. Rome.

Fofonoff, N. P., & Millard, R. C. (1983). Algorithms for computation of fundamental properties of seawater. *Unesco Technical Papers in Marine Science*, *44*, 1–53.

Freese, J., & Wing, B. (2003). Juvenile red rockfish, *Sebastes* sp., associations with sponges in the Gulf of Alaska. *Marine Fisheries Review*, *65*(3), 38–42.

Freiwald, A., & Roberts, J. M. (Eds.). (2005). *Cold-water corals and ecosystems*. Berlin: Springer-Verlag.

Furevik, T., & Foldvik, A. (1996). Stability at M_2 critical latitude in the Barents Sea. *J. Geophys. Res., 101(C4)*, 8,823-8,837.

Garau, B., Ruiz, S., Zhang, W. G., Pascual, A., Heslop, E., Kerfoot, J., & Tintoré, J. (2011). Thermal lag correction on Slocum CTD Glider data. *Journal of Atmospheric and Oceanic Technology*, *28*(9), 1065–1071. https://doi.org/10.1175/JTECH-D-10-05030.1

Gatti, S. (2002). The role of sponges in High-Antarctic carbon and silicon cycling - a modelling approach. *Ber. Polarforsch. Meeresforsch.*, *434*.

Genin, A., Dayton, P. K., Lonsdale, P. F., & Spiess, F. N. (1986). Corals on seamount peaks provide evidence of current acceleration over deep-sea topography. *Nature*, *322*(6074), 59–61. https://doi.org/10.1038/324148a0

Gilhousen, D. B. (1987). A field evaluation of NDBC moored buoy winds. *Journal of Atmospheric and Oceanic Technology*, *4*, 94–104.

Goldner, D. R., & Chapman, D. C. (1997). Flow and particle motion induced above a tall seamount by steady and tidal background currents. *Deep-Sea Research Part I: Oceanographic Research Papers*, *44*(5), 719–744. https://doi.org/10.1016/S0967-0637(96)00131-8

Haidvogel, D. B., Beckmann, A., Chapman, D. C., & Lin, R.-Q. (1993). Numerical simulation of flow around a tall isolated seamount. Part II: Resonant generation of trapped waves. *Journal of Physical Oceanography*, *23*(11), 2373–2391. https://doi.org/10.1175/1520-0485(1993)023<2373:NSOFAA>2.0.CO;2

Hansen, B., & Østerhus, S. (2000). North Atlantic-Nordic Seas exchanges. *Progress in Oceanography*, *45*(2), 109–208. https://doi.org/10.1016/S0079-6611(99)00052-X

Henkel, T. P., & Pawlik, J. R. (2005). Habitat use by sponge-dwelling brittlestars. *Marine Biology*, *146*(2), 301–313. https://doi.org/10.1007/s00227-004-1448-x

Herrnkind, W. F., Butler IV, M. J., Hunt, J. H., & Childress, M. (1997). Role of physical refugia: Implications from a mass sponge die-off in a lobster nursery in Florida. *Marine and Freshwater Research*, *48*(8), 759–770. https://doi.org/10.1071/MF97193

Hestetun, J. T., Tompkins-Macdonald, G., & Rapp, H. T. (2017). A review of carnivorous sponges (Porifera: Cladorhizidae) from the Boreal North Atlantic and Arctic. *Zoological Journal of the Linnean Society*, *181*(1), 1–69. https://doi.org/10.1093/zoolinnean/zlw022

Hoffmann, F., Radax, R., Woebken, D., Holtappels, M., Lavik, G., Rapp, H. T., … Kuypers, M. M. M. (2009). Complex nitrogen cycling in the sponge *Geodia barretti*. *Environmental Microbiology*, *11*(9), 2228–2243. https://doi.org/10.1111/j.1462-2920.2009.01944.x

Hogg, M. M., Tendal, O. S., Conway, K. W., Pomponi, S. A., van Soest, R. W. M., Gutt, J., … Roberts, J. M. (2010). *Deep-sea sponge grounds: Reservoirs of biodiversity. UNEP-WCMC Biodiversity Series No. 32.* Cambridge.

Hopkins, T. S. (1991). The GIN Sea - A synthesis of its physical oceanography and literature review 1972-1985. *Earth-Science Reviews*, *30*, 175–318.

Howell, K. L., Piechaud, N., Downie, A. L., & Kenny, A. (2016). The distribution of deep-sea sponge aggregations in the North Atlantic and implications for their effective spatial management. *Deep-Sea Research Part I: Oceanographic Research Papers*, *115*, 309–320. https://doi.org/10.1016/j.dsr.2016.07.005

Huthnance, J. M. (1989). Internal tides and waves near the continental shelf edge. *Geophysical & Astrophysical Fluid Dynamics*, *48*(1–3), 81–106.

Jeansson, E., Olsen, A., & Jutterström, S. (2017). Arctic Intermediate Water in the Nordic Seas, 1991–2009. *Deep-Sea Research Part I: Oceanographic Research Papers*, *128*(August), 82–97. https://doi.org/10.1016/j.dsr.2017.08.013

Kenchington, E., Power, D., & Koen-Alonso, M. (2013). Associations of demersal fish with sponge grounds on the continental slopes of the northwest Atlantic. *Marine Ecology Progress Series*, *477*, 217–230. https://doi.org/10.3354/meps10127

Klitgaard, A. B. (1995). The fauna associated with the outer shelf and upper slope sponges (Porifera, Demospongiae) at the Faroe Islands, Northeastern Atlantic. *Sarsia*, *80*(1), 1–22. https://doi.org/10.1530/EJE-11-0663

Klitgaard, A. B., & Tendal, O. S. (2004). Distribution and species composition of mass occurrences of large-sized sponges in the northeast Atlantic. *Progress in Oceanography*, *61*(1), 57–98. https://doi.org/10.1016/j.pocean.2004.06.002

Knudby, A., Kenchington, E., & Murillo, F. J. (2013). Modeling the distribution of *Geodia* sponges and sponge grounds in the Northwest Atlantic. *PLoS ONE*, *8*(12), 1–20. https://doi.org/10.1371/journal.pone.0082306

Kowalik, Z., & Proshutinsky, A. Y. (1993). Diurnal tides in the Arctic Ocean. *J. Geophys. Res.*, *98*(C9), 16,449-16,468.

Kulikov, E. A., Rabinovich, A. B., & Carmack, E. C. (2010). Variability of baroclinic tidal currents on the Mackenzie Shelf, the Southeastern Beaufort Sea. *Continental Shelf Research, 30*, 656-667. https://doi.org/10.1016/j.csr.2009.11.006

Kunze, E., & Sanford, T. B. (1986). Near-inertial wave interactions with mean flow and bottom topography near Caryn Seamount. *Journal of Physical Oceanography*, *16*(1), 109–120. https://doi.org/10.1175/1520-0485(1986)016<0109:NIWIWM>2.0.CO;2

Kunze, E., & Toole, J. M. (1997). Tidally driven vorticity, diurnal shear, and turbulence atop Fieberling Seamount. *Journal of Physical Oceanography*, *27*(12), 2663–2693. https://doi.org/10.1175/1520-0485(1997)027<2663:TDVDSA>2.0.CO;2

Kutti, T., Bannister, R. J., & Fosså, J. H. (2013). Community structure and ecological function of deep-water sponge grounds in the Traenadypet MPA - northern Norwegian continental shelf. *Continental Shelf Research*, *69*, 21–30. https://doi.org/10.1016/j.csr.2013.09.011

Kutti, T., Fosså, J. H., & Bergstad, O. A. (2015). Influence of structurally complex benthic habitats on fish distribution. *Marine Ecology Progress Series*, *520*, 175–190. https://doi.org/10.3354/meps11047

Leal, M. C., Puga, J., Serôdio, J., Gomes, N. C. M., & Calado, R. (2012). Trends in the discovery of new marine natural products from invertebrates over the last two decades - where and what are we bioprospecting? *PLoS ONE*, *7*(1). https://doi.org/10.1371/journal.pone.0030580

Leys, S. P., Yahel, G., Reidenbach, M. A., Tunnicliffe, V., Shavit, U., & Reiswig, H.M. (2011). The sponge pump: the role of current induced flow in the design of the sponge body plan. *PLoS ONE*, *6*(12). https://doi.org/10.1371/journal.pone.0027787

Lyard, F. H. (1997). The tides in the Arctic Ocean from a finite element model. *J. Geophys. Res.*, *102*(C7), 15,611-15,638.

Maldonado, M., Aguilar, R., Bannister, R. J., Bell, J. J., Conway, K. W., Dayton, P. K., … Young, C. M. (2015). Sponge grounds as key marine habitats: A synthetic review of types, structure, functional roles, and conservation concerns. In S. Rossi, L. Bramanti, A. Gori, & C. del Valle (Eds.), *Marine animal forests: The ecology of benthic biodiversity hotspots* (pp. 1–39). Cham: Springer International Publishing. https://doi.org/10.1007/978-3-319-17001-5_24-1

Mauritzen, C. (1996). Production of dense overflow waters feeding the North Atlantic across the

Greenland-Scotland Ridge. Part 1: Evidence for a revised circulation scheme. *Deep-Sea Research Part I: Oceanographic Research Papers*, *43*(6), 769–806.

McIntyre, F. D., Drewery, J., Eerkes-Medrano, D., & Neat, F. C. (2016). Distribution and diversity of deep-sea sponge grounds on the Rosemary Bank Seamount, NE Atlantic. *Marine Biology*, *163*(6), 1–11. https://doi.org/10.1007/s00227-016-2913-z

Mienis, F., De Stigter, H. C., White, M., Duineveld, G., De Haas, H., & van Weering, T. C. E. (2007). Hydrodynamic controls on cold-water coral growth and carbonate-mound development at the SW and SE Rockall Trough Margin, NE Atlantic Ocean. *Deep-Sea Research Part I: Oceanographic Research Papers*, *54*(9), 1655–1674. https://doi.org/10.1016/j.dsr.2007.05.013

Munk, W. H., & Phillips, N. (1968). Coherence and band structure of inertial motion in the sea. *Reviews in Geophysics, 6*, 447-472.

Murillo, F. J., Durán Muñoz, P., Cristobo, J., Ríos, P., González, C., Kenchington, E., & Serrano, A. (2012). Deep-sea sponge grounds of the Flemish Cap, Flemish Pass and the Grand Banks of Newfoundland (Northwest Atlantic Ocean): Distribution and species composition. *Marine Biology Research*, *8*(9), 842–854. https://doi.org/10.1080/17451000.2012.682583

Murillo, F. J., Kenchington, E., Lawson, J. M., Li, G., & Piper, D. J. W. (2016a). Ancient deep-sea sponge grounds on the Flemish Cap and Grand Bank, northwest Atlantic. *Marine Biology*, *163*(3), 1–11. https://doi.org/10.1007/s00227-016-2839-5

Murillo, F. J., Serrano, A., Kenchington, E., & Mora, J. (2016b). Epibenthic assemblages of the tail of the Grand Bank and Flemish Cap (northwest Atlantic) in relation to environmental parameters and trawling intensity. *Deep-Sea Research Part I: Oceanographic Research Papers*, *109*, 99–122. https://doi.org/10.1016/j.dsr.2015.08.006

New, A. L. (1988). Internal tidal mixing in the Bay of Biscay. *Deep Sea Research Part A, Oceanographic Research Papers*, *35*(5), 691–709. https://doi.org/10.1016/0198-0149(88)90026-X

Orvik, K. A., & Niiler, P. (2002). Major pathways of Atlantic water in the northern North Atlantic and Nordic Seas toward Arctic. *Geophysical Research Letters*, *29*(19), 2-1 - 2-4. https://doi.org/10.1029/2002GL015002

OSPAR. (2008). *OSPAR list of threatened and/or declining species and habitats (Reference number: 2008-6)*. London.

Pile, A. J., & Young, C. M. (2006). The natural diet of a hexactinellid sponge: Benthic-pelagic coupling in a deep-sea microbial food web. *Deep-Sea Research Part I: Oceanographic Research Papers*, *53*(7), 1148–1156. https://doi.org/10.1016/j.dsr.2006.03.008

Pitcher, T. J., Morato, T., Hart, P. J. B., Clark, M. R., Haggan, N., & Santos, R. . (Eds.). (2007).

Seamounts: Ecology, fisheries, and conservation. Oxford: Blackwell Publishing Ltd.

Plotkin, A., Gerasimova, E., & Rapp, H. T. (2017). Polymastiidae (Porifera: Demospongiae) of the Nordic and Siberian Seas. *Journal of the Marine Biological Association of the United Kingdom*. https://doi.org/10.1017/S0025315417000285

Proudman, J. (1916). On the motion of solids in a liquid processing vorticity. *Proceedings of the Royal Society of London*, *A92*, 408–424.

Pusceddu, A., Bianchelli, S., Martin, J., Puig, P., Palanques, A., Masque, P., & Danovaro, R. (2014). Chronic and intensive bottom trawling impairs deep-sea biodiversity and ecosystem functioning. *Proceedings of the National Academy of Sciences*, *111*(24), 8861–8866. https://doi.org/10.1073/pnas.1405454111

Rice, A. L., Thurston, M. H., & New, A. L. (1990). Dense aggregations of a hexactinellid sponge, *Pheronema carpenteri*, in the Porcupine Seabight (northeast Atlantic Ocean), and possible causes. *Progress in Oceanography*, *24*, 179–196.

Sandstrom, H. (1975). On topographic generation and coupling of internal waves. *Geophysical Fluid Dynamics*, *7*(1), 231–270.

Schneider, C. A., Rasband, W. S., & Eliceiri, K. W. (2012). NIH Image to ImageJ: 25 years of image analysis. *Nature Methods*, *9*(7), 671–675. https://doi.org/10.1038/nmeth.2089

Stoll, M. H. C., Bakker, K., Nobbe, G. H., & Haese, R. R. (2001). Continuous-flow analysis of dissolved inorganic carbon content in seawater. *Analytical Chemistry*, *73*(17), 4111–4116. https://doi.org/10.1021/ac010303r

Strickland, J. D. H., & Parsons, T. R. (1972). *A practical handbook of seawater analysis*. (J. C. Stevenson, J. Watson, J. M. Reinhart, & D. G. Cook, Eds.) (Second Edition). Ottawa: Fisheries Research Board of Canada.

Sundar, V. C., Yablon, A. D., Grazul, J. L., Ilan, M., & Aizenberg, J. (2003). Fibre-optical features of a glass sponge. *Nature*, *424*(6951), 899–900. https://doi.org/10.1038/424899a

Taylor, G. I. (1917). Motions of solids in fluids when the flow is not irrational. *Proceedings of the Royal Society of London*, *A93*, 99–113.

Torkildsen, M. M. (2013). *Diversity of hexactinellid sponges (Porifera, Hexactinellida) on an Arctic seamount, the Schultz Massif*. M.Sc. Thesis, University of Bergen.

van Haren, H., Hanz, U., De Stigter, H., Mienis, F., & Duineveld, G. (2017). Internal wave turbulence at a biologically rich Mid-Atlantic seamount. *PLoS ONE*, *12*(12), 1–16. https://doi.org/10.1371/journal.pone.0189720

van Weering, T., Koster, B., Van Heerwaarden, J., Thomsen, L., & Viergutz, T. (2000). New technique for long-term deep seabed studies. *Sea Technology*, *41*(2), 17–25.

Weatherall, P., Marks, K. M., Jakobsson, M., Schmitt, T., Tani, S., Arndt, J. E., … Wigley, R. (2015). A new digital bathymetric model of the world's oceans. *Earth and Space Science*, *2*, 331–345. https://doi.org/10.1002/2015EA000107

Wessel, P., & Smith, W. H. F. (1996). A global, self-consistent, hierarchical, high-resolution shoreline database. *Journal of Geophysical Research: Solid Earth*, *101*(B4), 8741–8743. https://doi.org/10.1029/96JB00104

White, M. (2003). Comparison of near seabed currents at two locations in the Porcupine Sea Bight - implications for benthic fauna. *Journal of the Marine Biological Association of the United Kingdom*, *83*(4), 683–686. https://doi.org/10.1017/S0025315403007641h

White, M., Bashmachnikov, I., Aristegui, J., & Martins, A. (2007). Physical processes and seamount productivity. In T. J. Pitcher, T. Morato, P. J. B. Hart, M. R. Clark, N. Haggan, & R. S. Santos (Eds.), *Seamounts: Ecology, fisheries, and conservation* (pp. 65–84). Oxford: Blackwell Publishing Ltd.

Whitney, F., Conway, K., Thomson, R., Barrie, V., Krautter, M., & Mungov, G. (2005). Oceanographic habitat of sponge reefs on the Western Canadian Continental Shelf. *Continental Shelf Research*, *25*(2), 211–226. https://doi.org/10.1016/j.csr.2004.09.003

Highlights – Oceanographic setting and short-timescale environmental variability at an Arctic seamount sponge ground (E.M. Roberts, F. Mienis, H.T. Rapp, U. Hanz, H.K. Meyer, A.J. Davies)

- Coinciding beneficial factors enhance sponge density and diversity at the seamount summit.
- The summit sponge ground occurred within nutrient-rich sub-surface water masses.
- It was regularly flushed with warmer, oxygen-enriched water from above.
- The suspended matter and current regime likely supplies food and prevents smothering.
- Mid-column lenses of elevated chlorophyll *a* indicate particle retention over the seamount.